LBNL-56483

ERNEST ORLANDO LAWRENCE
BERKELEY NATIONAL LABORATORY

Laser Sheet Light Flow Visualization For Evaluating Room Air Flows From Registers

Iain S. Walker Valerie Claret and Brian Smith

Environmental Energy Technologies Division

April 2006

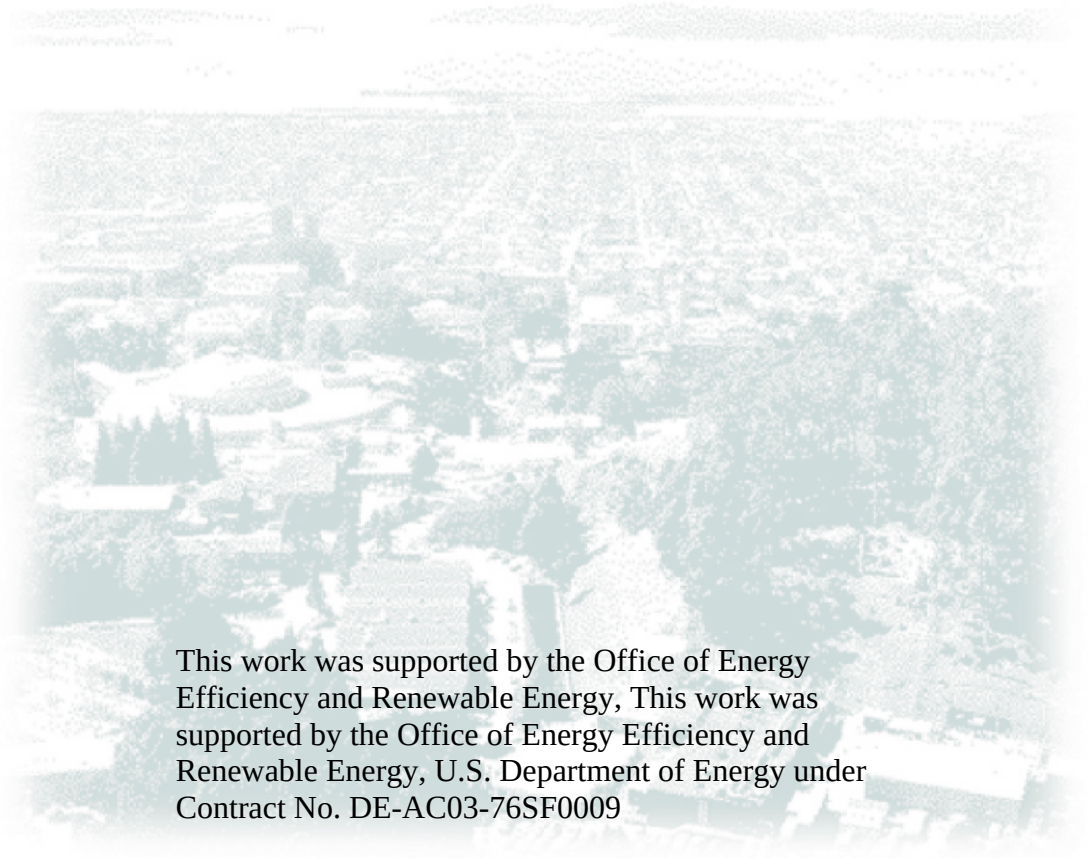

This work was supported by the Office of Energy Efficiency and Renewable Energy, This work was supported by the Office of Energy Efficiency and Renewable Energy, U.S. Department of Energy under Contract No. DE-AC03-76SF0009

Disclaimer

Introduction

Forced air heating and cooling systems and whole house ventilation systems deliver air to individual rooms in a house via supply registers located on walls ceilings or floors; and occasionally less straightforward locations like toe-kicks below cabinets. Ideally, the air velocity out of the registers combined with the turbulence of the flow, vectoring of air by register vanes and geometry of register placement combine to mix the supply air within the room. A particular issue that has been raised recently is the performance of multiple capacity and air flow HVAC systems. These systems vary the air flow rate through the distribution system depending on the system load, or if operating in a ventilation rather than a space conditioning mode. These systems have been developed to maximize equipment efficiency, however, the high efficiency ratings do not include any room mixing effects. At lower air flow rates, there is the possibility that room air will be poorly mixed, leading to thermal stratification and reduced comfort for occupants. This can lead to increased energy use as the occupants adjust the thermostat settings to compensate and parts of the conditioned space have higher envelope temperature differences than for the well mixed case. In addition, lack of comfort can be a barrier to market acceptance of these higher efficiency systems

To investigate the effect on room mixing of reduced air flow rates requires the measurement of mixing of supply air with room air throughout the space to be conditioned. This is a particularly difficult exercise if we want to determine the transient performance of the space conditioning system. Full scale experiments can be done in special test chambers, but the spatial resolution required to fully examine the mixing problem is usually limited by the sheer number of thermal sensors required. Current full-scale laboratory testing is therefore severely limited in its resolution. As an alternative, we used a water-filled scale model of a room in which whole-field supply air mixing maps of two vertical planes were measured using a Planar Laser-Induced Fluorescence (PLIF) measurement technique. Water marked with fluorescent dye was used to simulate the supply airflow; and the resulting concentrations within the water filled model show how the supply air mixes with the room air and are an analog for temperature (for thermal loads) or fresh air (for ventilation). In addition to performing experiments over a range of flow rates, we also changed register locations and examined the effects for both heating and cooling operation by changing the water density (simulating air density changes due to temperature changes) using dissolved salt.

Experimental apparatus

A 1:10 scale model of a 14’× 12’× 8’ (4.27m ×2.44m ×3.66m) room was constructed from aluminum and glass. The bottom had two glass-covered slots where the vertical planes of laser light entered the chamber. One slot was located along the centerline, the other near the front face of the model at a distance equivalent to 30 cm (1 foot) from the wall in full-scale. The front wall of the scale model was made from glass to allow observation of the room mixing flows. The room was empty with no internal partitions or obstructions to the flow.

To simulate the supply airflow, water containing a known concentration of fluorescent dye was introduced through an opening representing a supply register. Due to difficulties in

representing the small vanes common to residential registers in this scale model, the opening does not model any specific supply grille (i.e., 2-way or three way). Detailed laser Doppler anemometer measurements of the near flow field for residential register grilles by Tutu et al. (2003) has shown that the effect of grille directional vanes for both the mean and turbulent velocities profiles are negligible within a single register characteristic dimension. Therefore the elimination of the grille vanes should not result insignificant changes in jet development. The use of directional vanes that significantly alter the jet entering direction was not modeled in these tests and remains an area for future work.

The water exited the model room through a slot representing a door undercut. Both the supply and undercut were on the centerline of the room. The water/dye solution was pre-mixed in a 100 liter barrel and transported to the tank using a submersible pump. A gate valve was used to adjust each of the desired flow rates. Each flow rate was measured using a venturi-type flow meter (±0.5% manufacturers specified accuracy).

The sketch in Figure 1 shows these inlet and outlet locations within the test room.

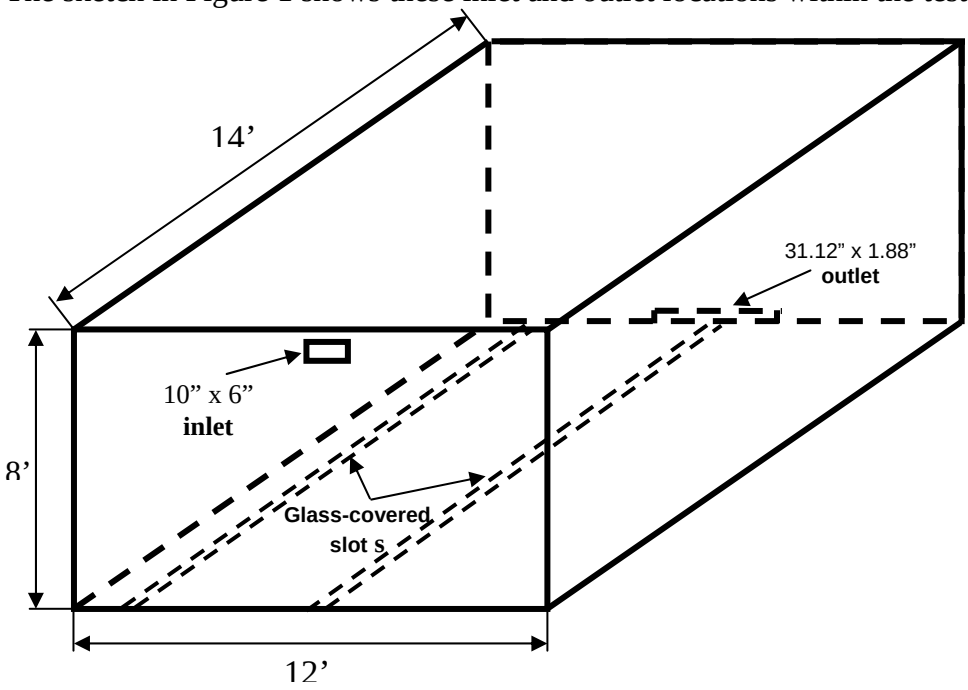

Figure 1: Sketch of the test room

A laser was directed through a set of optics to produce a sheet of light that was used to illuminate planes within the test room. This laser caused the dye to fluoresce so that the flow pattern could be observed at these planes. This measurement technique is known as Planar Laser-Induced Fluorescence (PLIF). During the experiment, pictures were recorded using a CCD video camera. The camera was linked to a microcomputer-based analog-to-digital converter that provided a gray level resolution of 256 values. This camera was specially selected to provide a linear response to light input (most video cameras are extremely non-linear). This linear response simplifies the analysis of the resulting images. The apparatus is illustrated in Figure 2. More details about the apparatus are given in Appendix 1. The level

of fluorescence varied with the concentration of the dye, so the light intensity at each pixel of the picture corresponded to the concentration of the supply water at this point. The pictures taken during the experiment were analyzed using a custom computer program developed specifically for this study[1]. An outline of this analysis program is given in Appendix 2.

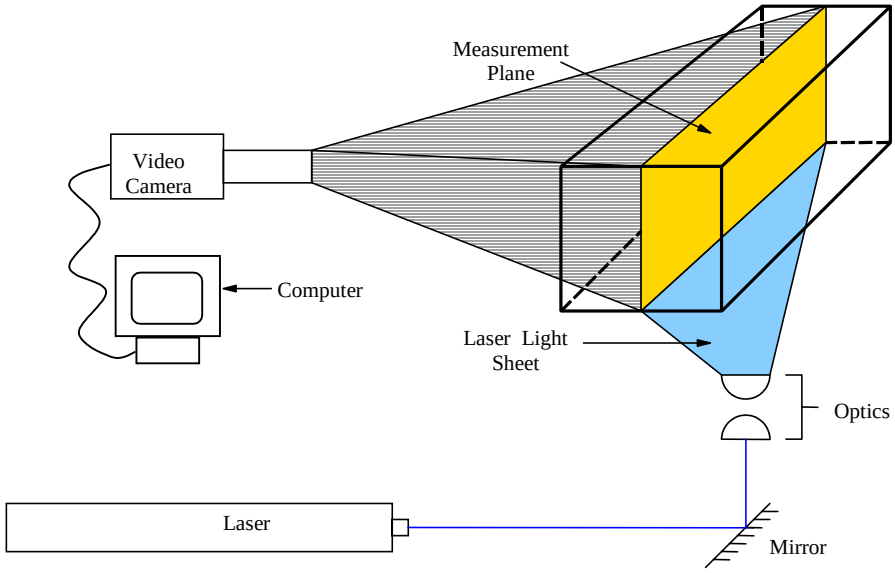

Figure 2: Illustration of PLIF apparatus

[1] Several commercially available image analysis packages were used, but their built-in features, such as auto zero and gain adjusting for each image, meant that they could not be used for our analyses.

Experimental Configurations

The following figures illustrate some of the test configurations used for heating and cooling experiments.

Cooling system:

High density fluid enters the room at a register near the top of the tank and leaves through a door undercut on the opposite side of the room

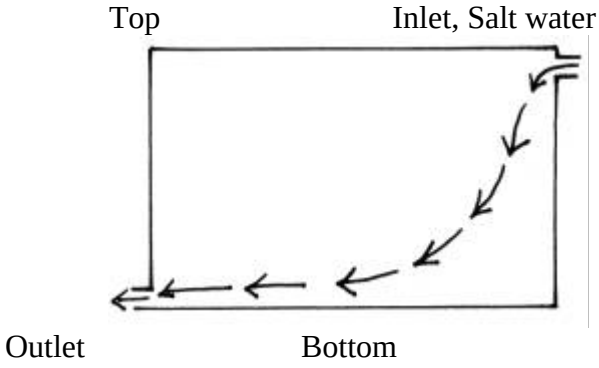

Figure 3. Cold air entering at high register – air exits through door undercut.

Heating system:

High density air or water enters a register near the bottom of the tank and leaves through a door undercut shaped exit at the top of the tank.

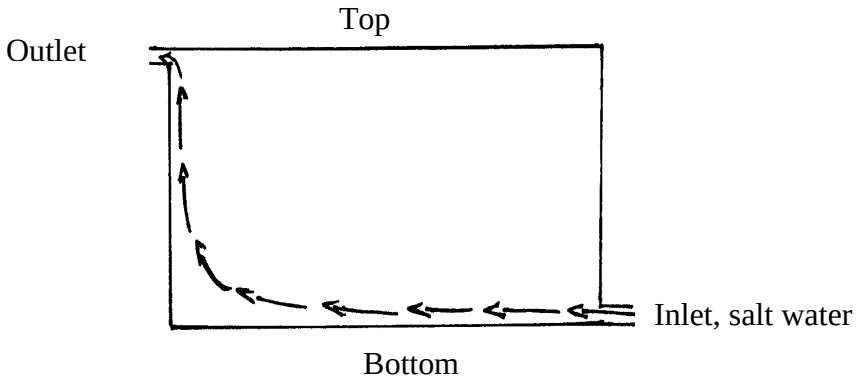

Figure 4. Experiment performed with higher density fluid – air enters low on wall and leaves via a high outlet

Inverting Figure 5 makes it look like a heating system with a high wall register:

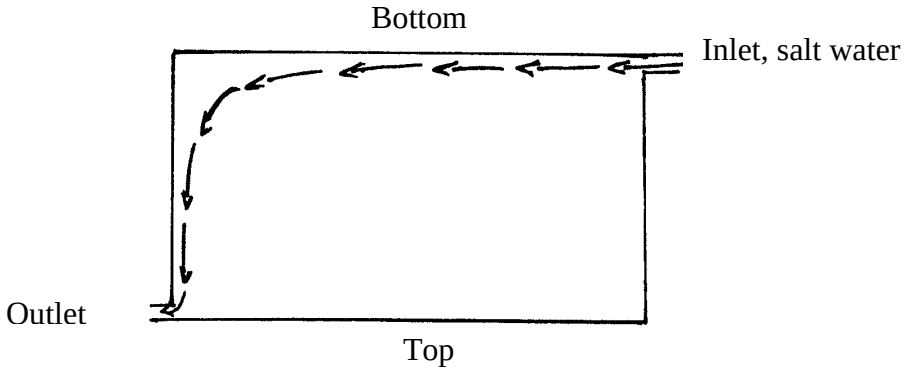

Figure 5. Inverted image of Figure 2 so that it resembles a high entry low exit heating system

Experimental Summary

For each system configuration of inlets and outlet location, three different supply flow rates were simulated: 25 cfm, 50 cfm and 100 cfm. These flow rates cover a reasonable range for a room of this size. For each flow rate, three to five experiments were performed and averaged to account for the stochastic run-to-run variability. The experiments were performed until the total volume of water that entered the tank was equal to the volume of the tank, i.e., one air change. Note that this does not mean that all the water originally in the tank at the start of the experiment has been displaced. A step-by-step procedure of the experiments can be found in Appendix 2.

To provide a uniform basis for comparison between the test configurations, flow rates and fluid densities, we focused our study on specific locations within the tank. Figure 6 shows the location of the nine locations studied. These areas were chosen to encompass the locations within a room that would be occupied by standing or sitting individuals (i.e., the head and ankle locations discussed above). Each square measures 0.475m x 0.475m (18.7”x18.7”) in full scale. The occupied zone is up to 1.7 m (5.58’) from the floor. The measured concentrations were averaged for each square for every image analyzed. Details of the image analysis are given in Appendix 3.

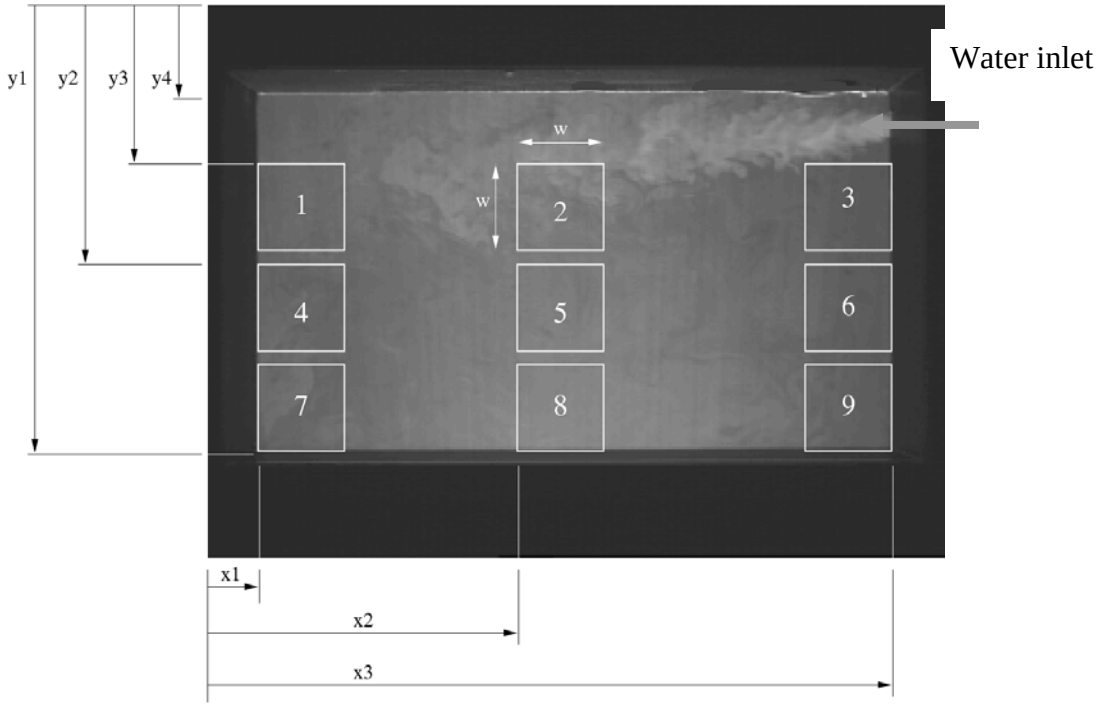

Figure 6: Side view of model showing the locations of nine squares used in the analysis superimposed over a sample test image

For experiments taking images on the centerline the locations are:

W	X1	X2	X3	Y1	Y2	Y3	Y4
30	21	143	295	192	124	85	38

For experiments taking pictures close to the front wall:

W	X1	X2	X3	Y1	Y2	Y3	Y4
33	11	142	307	197	122	80	29

Scale modeling of room air flows

We used standard similarity theory relationships to convert between full-scale and model parameters. Much of the following analysis is based on Thatcher et al. (2002). These relationships require the following scales in terms of physical dimensions and flow rates.

Mean Length Scales:

$$L_{inlet} \equiv A_{inlet}^{\frac{1}{2}} \qquad (1)$$
$$L_{room} \equiv V_{room}^{1/3}$$

Mean Velocity Scales:

$$U_{inlet} \equiv Q_{inlet}/A_{inlet} \qquad (2)$$
$$U_{room} \equiv Q_{inlet}/V_{room}^{2/3}$$

Residence Times:

$$t_{inlet} \equiv A_{inlet}^{3/2}/Q_{inlet} \qquad (3)$$
$$t_{room} \equiv V_{room}/Q_{inlet}$$

Where:
L = characteristic length
A = Area
V = Volume
U = Velocity
T = time
Q = volumetric flow rate

Based on these definitions, the mean flow Reynolds numbers can be defined as follows.

$$\mathrm{Re}_{inlet} = \frac{U_{inlet} L_{inlet}}{\nu_{inlet}} = \frac{Q_{inlet}}{A_{inlet}^{1/2} \nu_{inlet}} \qquad (4)$$

$$\mathrm{Re}_{room} = \frac{U_{room} L_{room}}{\nu_{room}} = \frac{Q_{inlet}}{V_{room}^{1/3} \nu_{room}} \qquad (5)$$

Where ν_{inlet} and ν_{room} are the kinematic viscosities for the fluids: water for the reduced scale model and air for the full-scale room. To make the inlet jets Reynolds number equivalent for both the full scale and the model scale:

$$\frac{Q_{inlet,\,full}}{A_{inlet,\,full}^{1/2} \nu_{air}} = \frac{Q_{inlet,\,model}}{A_{inlet,\,model}^{1/2} \nu_{water}} \qquad (6)$$

For the room flow this condition is met if:

$$\frac{Q_{inlet,\,full}}{V_{room,\,full}^{1/3}\nu_{air}} = \frac{Q_{inlet,model}}{V_{room,model}^{1/3}\nu_{water}} \qquad (7)$$

Substituting the defined length and velocity scales into these equations gives the required flow ratio:

$$\frac{Q_{\,inlet\ \ ,\,full}}{Q_{\,inlet\ \ ,model}} = \left(\frac{L_{\,full}}{L_{\,model}}\right)\left(\frac{\nu_{\,air}}{\nu_{\,water}}\right) \qquad (8)$$

The length scale ratio is 10 and the ratio of the kinematic viscosities of air to water is approximately 16 (at 20° C), and therefore the ratio between the full flow and the model flow is a factor of 160. The test flows are 25 cfm, 50 cfm and 100 cfm at full scale, therefore the model flows are: 0.156 cfm, 0.313 cfm, and 0.625 cfm (0.265 m^3/h, 0.53 m^3/h and 1.06 m^3/h) respectively.

The time scale between full scale and the model can be determined from the time scale definitions as follows:

$$\frac{t_{\,room\ \ ,\,full}}{t_{\,room\ \ ,model}} = \frac{\left(\frac{V_{\,room\ \ ,\,full}}{Q_{\,inlet\ \ ,\,full}}\right)}{\left(\frac{V_{\,room\ \ ,model}}{Q_{\,inlet\ \ ,model}}\right)} = \left(\frac{L_{\,room\ \ ,\,full}}{L_{\,room\ \ ,model}}\right)^3\left(\frac{Q_{\,inlet\ \ ,model}}{Q_{\,inlet\ \ ,\,full}}\right) \qquad (9)$$

For the 10:1 scale model used in these experiments and the flow rate ratio of 160 we have a time scale ratio of 6.25. In others words, one second of flow for the model would simulate 6.25 seconds of flow for the full-scale room. With images captured at a rate of about 1.7 times a second, each image represents about 3.7 seconds of real time flow.

Scale modeling of buoyancy

To simulate heating or cooling conditions, (i.e. the distribution of hotter or colder air within the room) the key fluid property change is density. The change in air density with temperature is modeled by mixing water with salt to increase water density. For cooling, the increased density is directly related to the increase air density for cold supply air. For heating, the original plan was to mix water supply with ethyl alcohol to reduce water density. However, this method would require the use of large quantities of alcohol: about 1.5 m^3 of alcohol for 1 m^3 of water to achieve the required density ratios. Therefore the ethyl alcohol option was abandoned for reasons of cost and safety. The heating air flow patterns were therefore obtained by inverting the images obtained for cooling simulations. This has the effect of reversing the register locations, i.e., a high supply register cooling experiment looks like a low wall register heating experiment. This limits the density difference we can model to be the same in heating and cooling. So the results for heating are suitable for a heat pump (with delivery temperatures below 32°C (90°F)), but not for furnaces with their higher delivery temperatures and therefore greater air density differences.

For the scale model to exactly represent the effects of buoyancy and inertial forces in the full size room, it is necessary to match the Richardson number (Ri). The following calculations were used to determine the salt solution concentrations required for the experiments.

$$Ri = \frac{g\Delta TL}{TU^2} \tag{10}$$

or

$$Ri = \frac{g\Delta\rho L}{\rho U^2} \tag{11}$$

So for equal model and full scale Ri:

$$\frac{\Delta\rho_{model}}{\rho_{model}} = \frac{\Delta\rho_{full}}{\rho_{full}} \frac{L_{full}}{L_{model}} \frac{U_{model}^2}{U_{full}^2} \tag{12}$$

The velocity scales are:

$$U = \frac{Q}{A} = \frac{Q}{L^2} \tag{13}$$

Equations (12) and (13) give:

$$\frac{\Delta\rho_{model}}{\rho_{model}} = \frac{\Delta\rho_{full}}{\rho_{full}} \frac{Q_{model}^2}{Q_{full}^2} \frac{L_{full}^5}{L_{model}^5} \tag{14}$$

With length and velocity scales fixed, this equation fixes the density ratio of our experiment. As shown before, our model flow rate is 160 times higher than full scale and the length scale factor is 10. So we have:

$$\frac{\Delta\rho_{model}}{\rho_{model}} = \frac{\Delta\rho_{full}}{\rho_{full}} \frac{1}{160^2} \frac{10^5}{1} = 3.9 \frac{\Delta\rho_{full}}{\rho_{full}} \tag{15}$$

For the cooling system experiments we simulated a 10° C temperature difference. Room air temperature is 26°C (299K) and the supply air is 16°C (289 K). Using the density ratio to simulate the inverse of the temperature ratio, it follows that:

$$\frac{\rho_{inlet}}{\rho_{room}} = \frac{T_{room}}{T_{inlet}} = \frac{299\ K}{289\ K} = 1.0346 \tag{16}$$

Therefore,

$$\frac{\rho_{inlet} - \rho_{room}}{\rho_{room}} = (1.0346 - 1) = 3.46\% \quad (17)$$

The ratio of the density difference of supply and room air to room density is about 3.46%. Our Ri analysis showed that the ratio required in the model is 3.9 times that of full scale. Therefore, the density of the salt water required is 13.5% higher than the density of fresh water. The density of water at 20°C and atmospheric pressure is 998 kg/m^3. Therefore the target salt water density is 998 kg/m^3 × 1.1349=1132 kg/m^3. Tests were carried out to determine the quantity of salt necessary to be added in order to obtain the appropriate density. Those tests were performed using a hydrometer (specific gravity for heavy liquids, range 1.000-1.220, precision 0.002), and we found that 210 g of salt per liter were required. For each experiment 21 kg (46.3 pounds) of salt was required to get the appropriate density for a 100 liter barrel (26.4 gallons) of pre-mixed dye/water/salt solution.

Calibrating the PLIF system

Laser Sheet Non-Uniformity Correction

First, an image is taken with just fresh water as a baseline to account for the initial conditions (e.g. ambient light). Every subsequent image will have this baseline image subtracted before further processing. The next step is to find the relationship between the measured light intensity at a pixel and the concentration of supply water. The supply water contains a known concentration of fluorescent dye. In our experiment we used a dye concentration of 80 μg per liter. The dye florescence intensity emitted at each pixel location is directly proportional to the local dye concentration and the local intensity of the laser light.

$$I = C \cdot E \cdot A \cong C \cdot E \quad (18)$$

Where:
I = the level of fluorescence intensity
C = the concentration of the dye
E = the laser light intensity
A = Absorption factor to account for light absorption along its path (≈ 1 at low dye concentrations)

The challenge is that the relatively small cylindrical lenses used in our experiment spread the laser beam in such a manner that the intensity of the laser light in the plane was not uniform. The light intensity was greatest at the bottom center and decreased towards the top and the sides (as illustrated in Figure 7). The “rays” in figure 7 were due to a combination of lens distortions, small dust particles on the optics and tank surfaces and flaws in the glass tank insert that the sheet shines through.

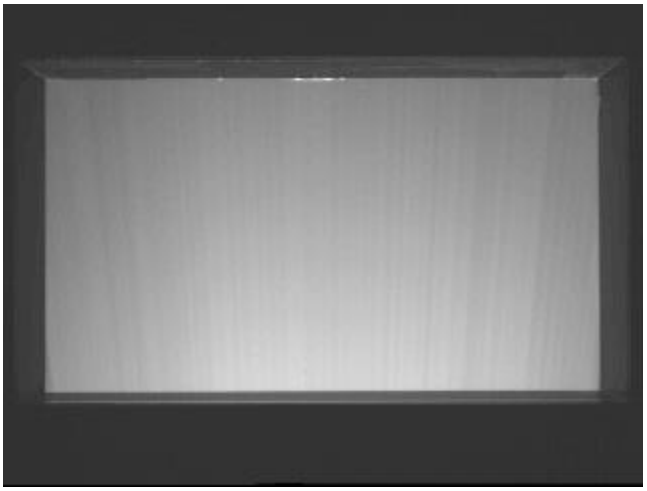

Figure 7: Distribution of laser light intensity with uniform dye concentration

To correct for this non-uniformity of the laser sheet, a reference baseline picture was taken with the dye at a known uniform concentration. All the experimental images were divided by this reference picture using the image processing software, i.e., the measured intensity at each pixel of a picture is divided by the measured intensity at the same pixel obtained from the reference picture. The second step in this correction was to multiply each the experimental image by the mean intensity value of the calibration picture.

$$\frac{I_{x,y}}{I_{cal,x,y}} * mean\ (I_{cal}) = I_{correct\ ,x,y}$$

This correction was performed for all images taken during the experiments.

Calibrating light intensity to dye concentration

To determine the relationship between the intensity and the concentration of supply water, images of the model filled with different known dye concentrations were recorded. The dye was mixed outside the tank in a separate 26.4 gallon (100L) barrel. A single known concentration was mixed in the barrel and pumped into the tank. The mean light intensity of each calibration image was measured. Then the intensity obtained was compared to the ratio of the corresponding dye concentration and the dye concentration used for the actual experiments (80μg/L). Typically, calibration images were obtained from 0% to 100% (of the supply 80μg/L) in 10% steps. These calibrations were repeated for two cases: along the centerline of the tank, and with the beam shining through the near wall aperture. It was important to obtain the calibration data at both positions to account for light absorption by the water/dye/salt mixture on the path between the sheet of laser light and the glass front of the tank. The calibration data were used to produce a relationship that links the light intensity to the fraction of supply water concentration. The relationship is almost linear, as illustrated in Figure 8. A second order polynomial was found to fit the calibration data well, with an RMS error of 1.5%:

$$C = 0.0013I^2 + 0.6014I \qquad (19)$$

Note that this is different from the ideal linearized Equation 18.

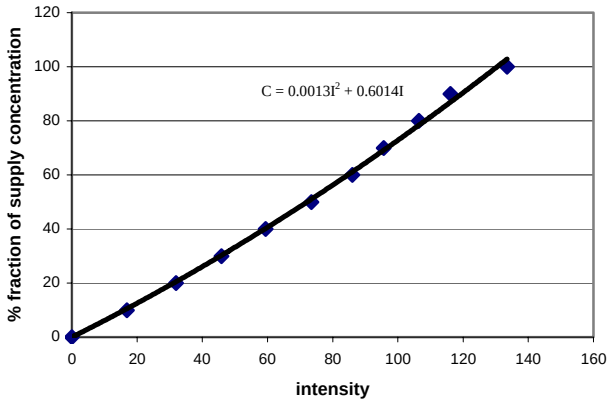

Figure 8: Calibration curve at the centerline with no salt

Because the calibration was found to be sensitive to small changes in the laser beam (due to alignment changes between the laser beam, mirror and lenses, combined with slight changes in laser power output), it is repeated every time the tank is moved when changing the laser position from centerline to near the wall and vice versa.

For tests using salt water, the calibrations were prepared differently because salt water and pure water were found to have different absorption of the laser light. The differences are apparent in the calibration curve equations shown in the following table. For the near-wall case, the light from the light sheet only travels through a little of the tank and is unaffected. However, the centerline results show significant absorption, as shown by the calibration results in Table 1. Therefore we used location specific calibrations: centerline for centerline experiments and near-wall results for near-wall experiments.

Table 1. Comparison of PLIF Calibrations for pure water and salt water

	Centerline equation	Wall equation
Pure water	$C=0.0013I^2+0.6014$	$y=0.0013I^2+0.5814I$
Water/salt mixing	$C=0.0024I^2+0.6054I$	$C=0.0013I^2+0.5941I$

Human thermal comfort

The principal purpose of heating, ventilating and air-conditioning system is to provide conditions for human thermal comfort. A widely accepted definition is, “Thermal comfort is that condition of mind that expresses satisfaction with the thermal environment” (ASHRAE standard 55). We focused our interest on the effect of a vertical air temperature difference. In most spaces in buildings, the air temperature normally increases with height above the floor.

If the gradient is sufficiently large, local warm discomfort can occur at the head and/or cold discomfort can occur at the feet, although the body as a whole is thermally neutral.

Chapter 8 of the ASHRAE Handbook of Fundamentals (2001) summarizes several studies of vertical air temperature differences and the influence of thermal comfort by Olesen et al (1979), McNair (1973) and McNair and Fishman (1974). Subjects were seated in a climatic chamber and individually exposed to different air temperature differences between head and ankles (Olesen et al.1979). During the test, the subjects were thermally neutral because they were allowed to change the temperature level in the test room whenever they desired; the vertical temperature difference, however, was kept unchanged. The subjects gave subjective reactions to their thermal sensation. Figure 9 shows the percentage of dissatisfaction as a function of the vertical temperature difference between the head (1.1 m above the floor) and ankles (0.1 m above the floor). We used this information to assess the thermal comfort for each experiment based on the temperature difference between head and ankle locations within the model.

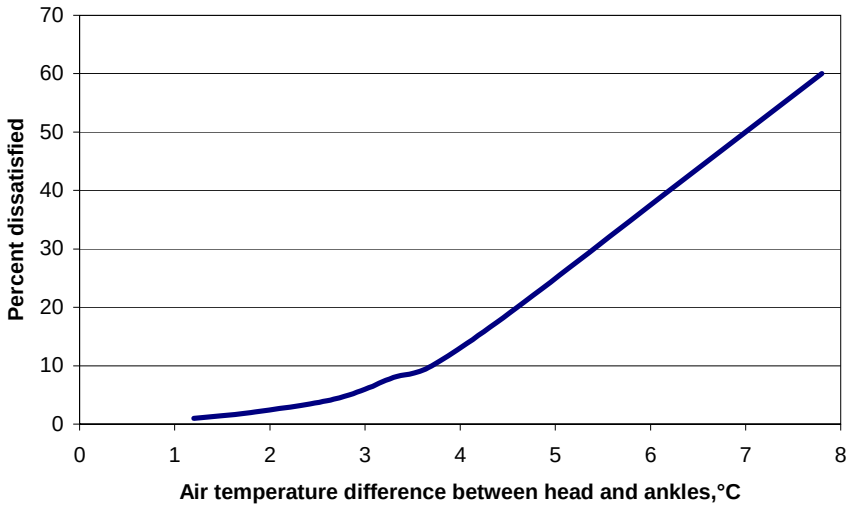

Figure 9: Percentage of Seated People Dissatisfied as Function of Air Temperature Difference Between Head and Ankles

Test Results

For each test configuration the following results will show example images together with plots showing concentration changes with time. The dye concentration corresponds to fraction of fresh air for ventilation simulations, where zero percent corresponds to original room air and 100% is outside air only. Similarly for heating and cooling cases, the concentration is a surrogate for temperature, where zero percent is the initial room temperature and 100% is the supply air temperature (the difference being 10°C in these experiments).

Ventilation

For ventilation simulations, the water and dye solutions have no added salt and are the same density as the water in the tank. The inlet was located at the top of the tank with the outlet at the bottom. Observations of flow patterns for all three experiments were similar as shown in the centerline images in Figure 10.

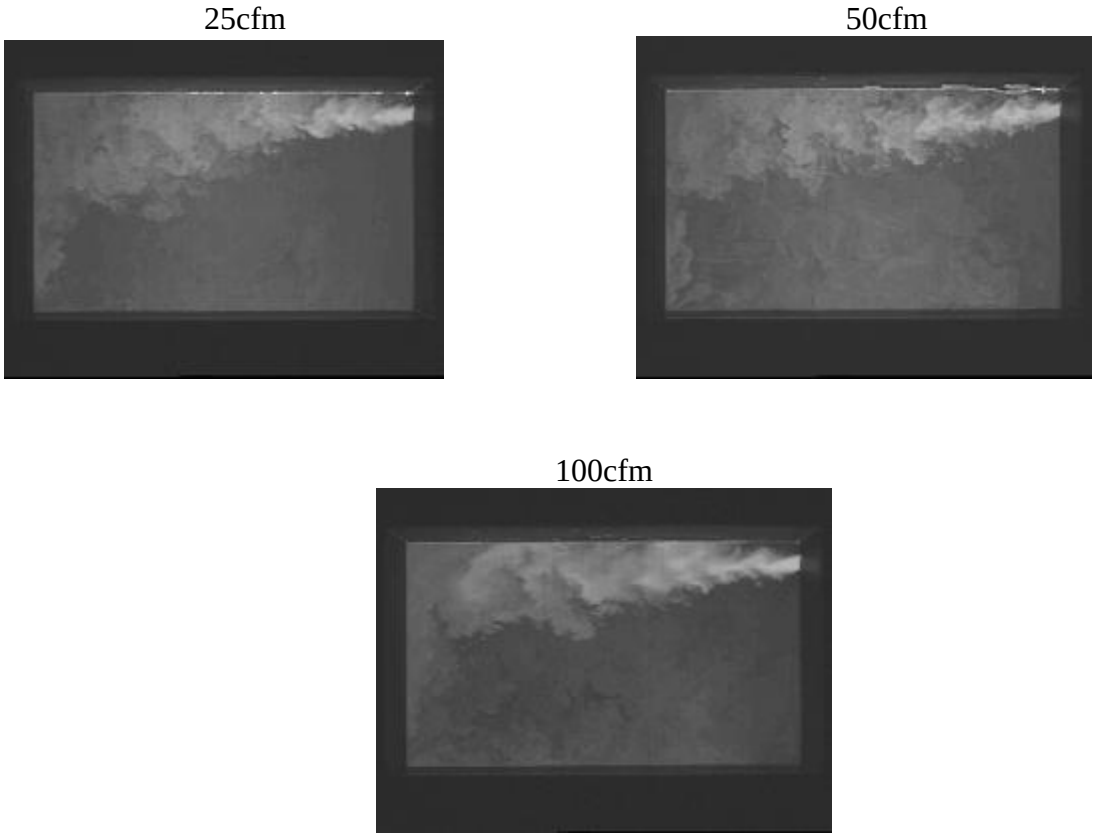

Figure 10: Example centerline images for neutrally buoyant ventilation simulations

Figure 11 shows the evolution of the mean dye concentration in squares 1, 2 and 3 (at approximately head height for a standing person - see Figure 6 for locations) for different flow rates at the centerline. These squares are at the same height but positioned at decreasing

distances from the inlet register. For comparison purposes, the concentration development curve for perfect mixing has been included in the figures. In the perfect mixing case, the dye would immediately mix with all the water in the tank resulting in a uniform dye concentration throughout the tank, and the dye concentration within the tank and the dye concentration at the tank outlet are the same. More details on the calculation of the perfect mixing concentrations are given in Appendix 5. The concentration results for all the sample regions in the tank for all the experiments are given in Appendix 6.

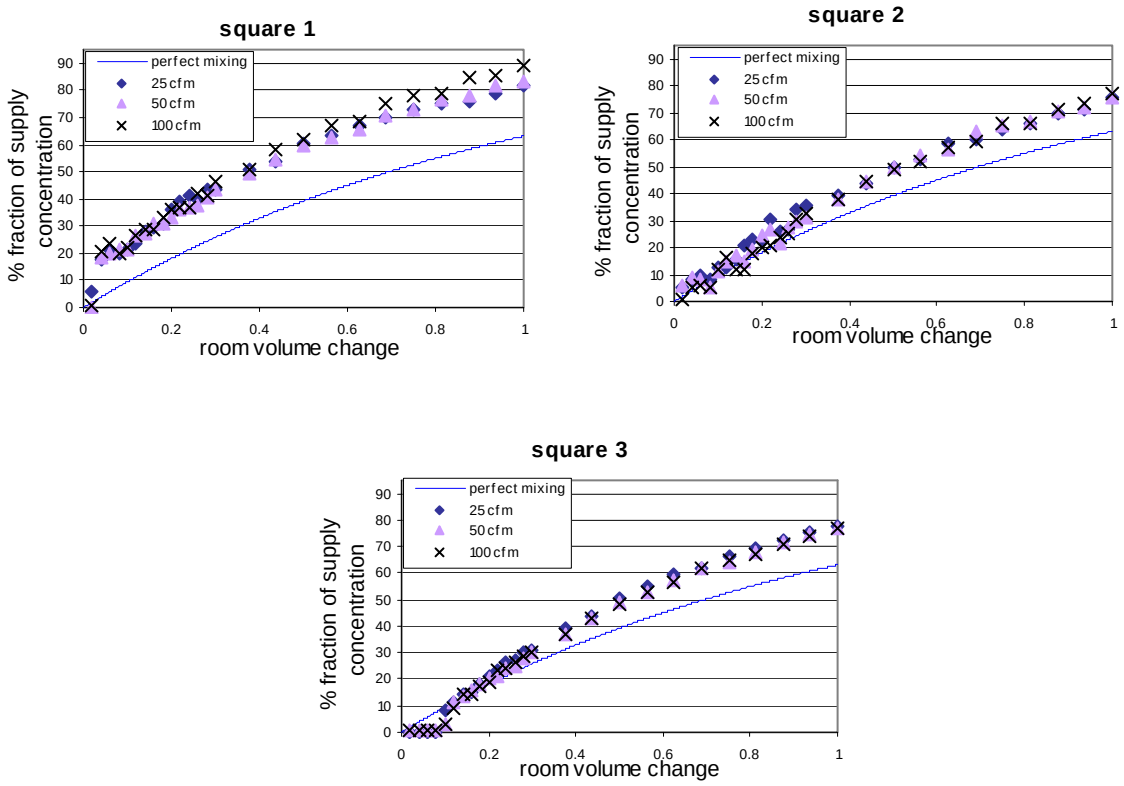

Figure 11: Ventilation simulation, centerline, squares 1,2 and 3

The results show that almost all points are higher than the perfect mixing curve. This is due to the three-dimensional nature of the flow. Looking down into the tank we observed the flow pattern sketched in Figure 12. The jet region is at the centerline and the dye concentration remains higher in this region than in other regions of the tank. The jet strikes the far wall and then flows back along the walls – leaving a region inbetween the centerline and walls that is not well mixed with the main flow.

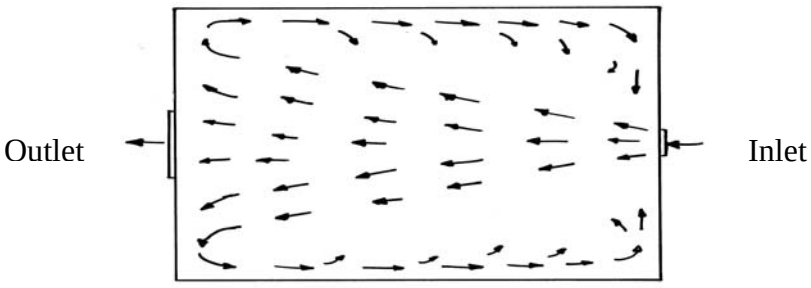

Figure 12: Sketch of the flow pattern, plan view

The differences between concentrations for a given volumetric air exchange for the three flow rates are small (less than 10 %), but the flow rate of 100 cfm provided slightly higher concentrations. These results indicate that rates of 25 cfm or higher should be sufficient to obtain reasonable mixing within the room at head height for a standing person. Square 1 had higher concentrations than those in others areas because the jet flowed directly through this square, whereas it flowed mostly over the top of squares 2 and 3.

There was a time delay before any dye was observed within each sample square. The time delay is the time taken for the flow to travel from the register to the sample square. The timing starts when the register is opened at the beginning of the experiment. This time delay varies depending on flow rate and square location within the tank. Details of the time delay calculations are provided in Appendix 4. As shown in Table 2, in the worst case, it takes about three minutes for the supply air to reach the entire occupied zone in the centerline. Time delays were higher for squares 3, 6 and 9 for the lower flow rates. For the 100 cfm flow rate there were time delays in all squares except the square 1 because the jet flowed through this square as soon as the register was opened.

Table 2: Ventilation simulation time delays, centerline

Square	Full scale time delay 25 cfm	Full scale time 50 cfm	Full scale time 100 cfm
1	No delay	No delay	No delay
2	No delay	12 sec	23 sec
3	2 min 30 sec	1 min 24 sec	41 sec
4	No delay	No delay	12 sec
5	1 min 48 sec	1 min 12 sec	44 sec
6	2 min 36 sec	1 min 18 sec	39 sec
7	48 sec	24 sec	34 sec
8	2 min 12 sec	1 min 12 sec	46 sec
9	3 min 12 sec	1 min 30 sec	13 sec

Figure 13 shows the evolution of the mean dye concentration in squares 1, 2 and 3 for different flow rates near the wall. These squares are representatives of others levels (4, 5, 6 and 7, 8, 9).

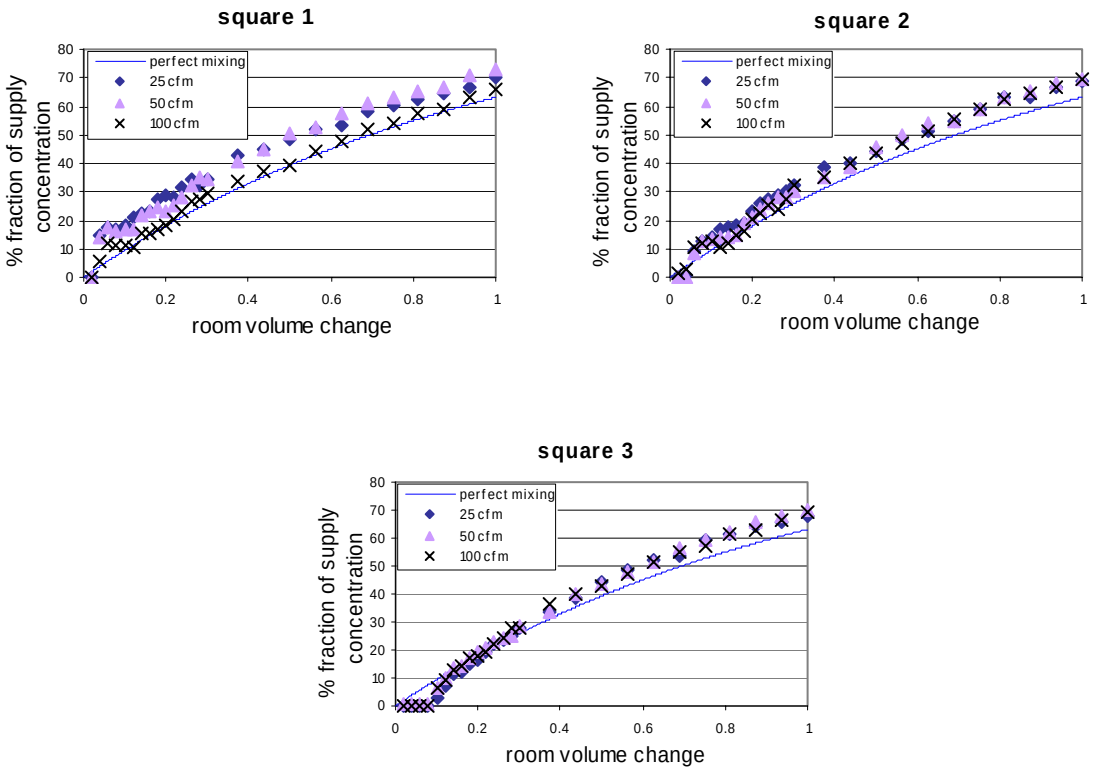

Figure 13: Ventilation simulation, near wall, squares 1, 2 and 3

As observed during the centerline experiments, nearly all concentrations were higher than for perfect mixing. This is because the flow enters the room along the centerline, and after striking the far wall it flows around the edges of the room. This means that both the centerline and near wall data will tend to have high concentrations compared to the region between them that was not examined in our experiments. For these near-wall experiments the differences in concentrations for different flow rates were also less than 10%. Figure 14 compares the centerline and near wall results for square 4. As expected, the centerline concentrations were higher than those near the wall because the jet has had longer to mix with the rest of the room as it flows back along the wall.

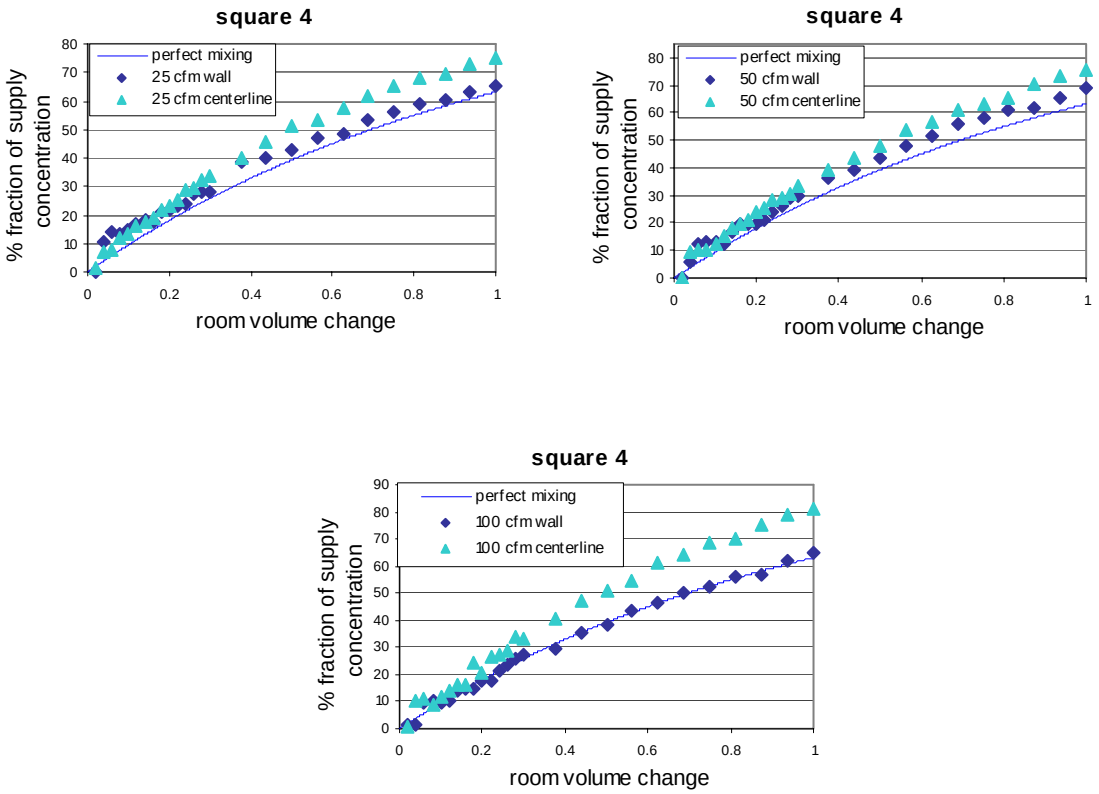

Figure 4: Ventilation simulation. Comparison of centerline and near wall results.

Table 3 summarizes the time delays for these near wall locations. The time delays near the wall were shorter than time delays observed at the centerline. Again, this is due to the circulation pattern inside the room. As the jet hits the wall opposite the inlet, it then diverts back along the sidewall and reaches square 3, 6 and 9 sooner near the wall than at the centerline. The long time delay for Square 1 is due to there being little flow in this high corner region.

Table 3: Time delays, Ventilation simulation, near the wall			
Square	Full scale time delay 25 cfm	Full scale time 50 cfm	Full scale time 100 cfm
1	4 min 12 sec	No delay	No delay
2	No delay	6 sec	No delay
3	2 min 42 sec	1 min	32 sec
4	No delay	No delay	No delay
5	No delay	6 sec	No delay
6	2 min 24 sec	1 min	24 sec
7	No delay	No delay	No delay
8	No delay	No delay	No delay
9	3 min	1 min	24 sec

Summary of Ventilation Simulation Results

The test results showed that that there were no significant differences in fresh air concentrations between the three flow rates used in the experiment, except for the time taken for the air flow to reach a given location at start-up. If the system being modeled has a ten minute working cycle, nearly the half time is required to reach all the squares with the 25 cfm flow rate (4 min 12 sec for square 1 near the wall). So for this ventilation system, the 50 cfm or 100 cfm flow rate would be preferred.

Cooling

High inlet

The inlet was located at the tank top, the outlet at the bottom. The images in Figure 15 show that the flow patterns for each of the cooling simulation experiments were not the same and also differed from the ventilation system simulations.

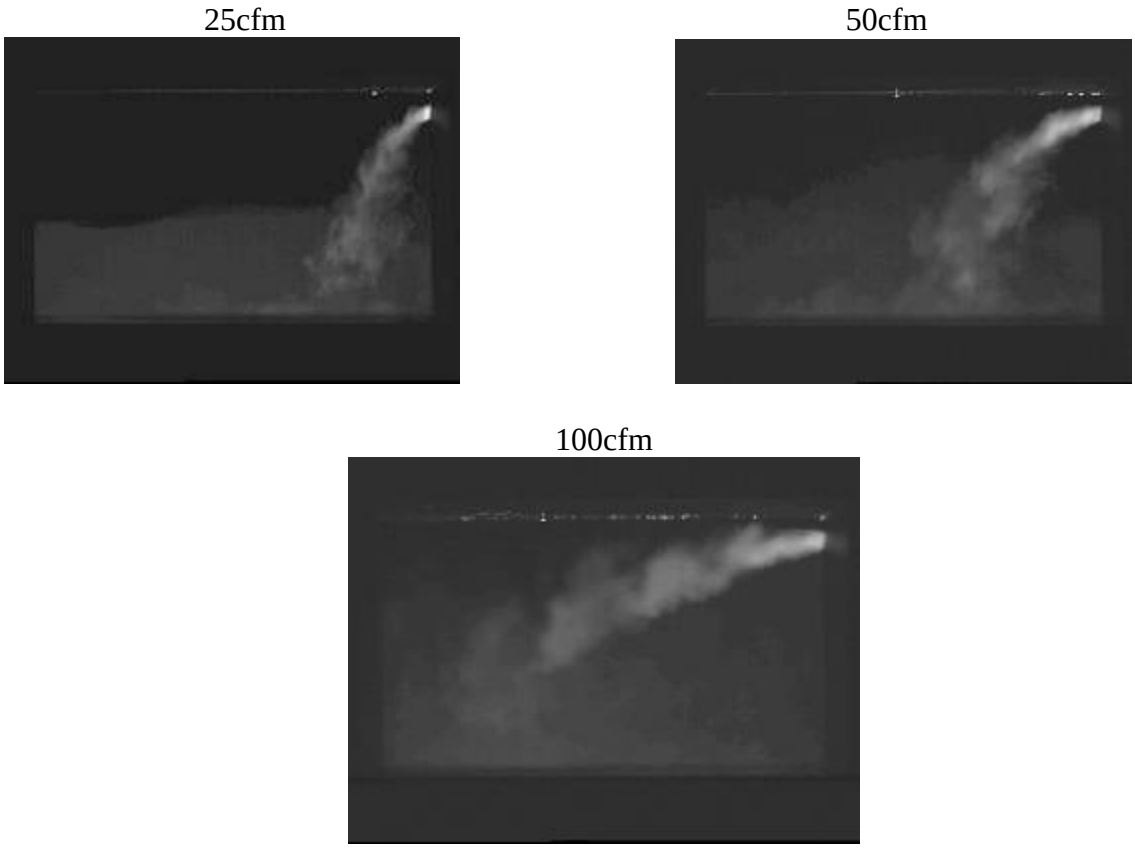

Figure 15. Cooling centerline example images for high inlet

At lower flow rates, the negative buoyancy of the cold jet had more impact than the initial velocity of the jet and the jet falls down toward the floor. For the 100 cfm flow rate the jet form appeared to be a closer match to the ventilation case. Also, the lower flow rates have visible stratification with a layer of cold air near the floor that does not mix with the air higher up in the room. Another observation is (as shown in Figure 16) that the final concentrations for the cooling system experiments were lower than those obtained for the ventilation system simulation. This is because the flow pattern with the strongly negatively buoyant cold jet resulted in a decrease in mixing and significant stratification. Because the outlet was on the bottom of the tank, the concentration of supply air in the outlet flow was higher than the discharge for the ventilation system case, resulting in lower concentration fluid left in the tank.

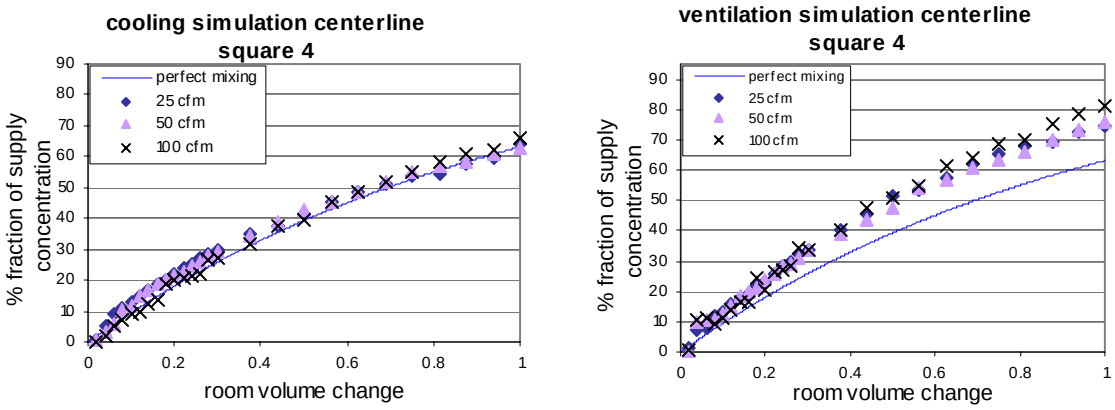

Figure 16. Comparison of Cooling and Ventilation Simulations

Observations at the centerline:

Figure 17 shows the evolution of the mean dye concentration in squares 1, 2 and 3 for different flow rates at the centerline. In square 2 for the 100 cfm flow rate, the dye concentration change was irregular. The supply jet appeared intermittently in this square, sometimes flowing through it and not at other times. In squares 5 and 8, the 50 cfm flow rate produced uniformly higher concentrations because the jet flowed directly through these two squares.

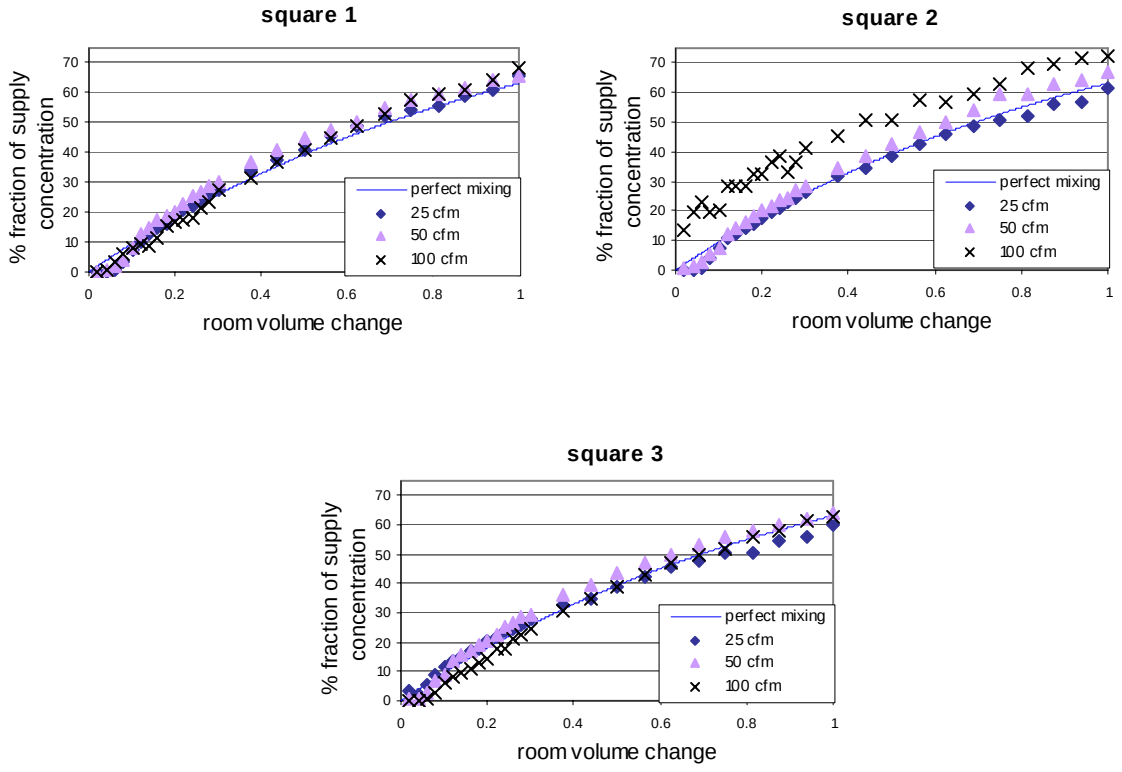

Figure 17: Cooling simulation, centerline, high inlet, squares 1, 2 and 3

Table 3 summarizes the time delay for the cooling experiments. Because the jet falls toward the occupied zone the time delays were lower in the cooling system simulation than those in the ventilation system simulation. Time delays for flow rates 25 cfm and 50 cfm show that there is a stratification phenomenon because areas at the top of the occupied zone were reached last. For the 100 cfm flow rate, the greater mixing meant that the stratification was not apparent in the occupied zone.

Table 3. Time delays on the centerline for cooling simulations and a high inlet

Square	Full scale time delay 25 cfm	Full scale time 50 cfm	Full scale time 100 cfm
1	1 min 18 sec	24 sec	30 sec
2	49 sec	28 sec	No delay
3	No delay	5 sec	34 sec
4	No delay	No delay	11 sec
5	No delay	No delay	No delay
6	No delay	No delay	34 sec
7	No delay	No delay	No delay
8	No delay	No delay	5 sec
9	No delay	No delay	30 sec

Observations near the wall

Figure 18 shows the evolution of the mean dye concentration in squares 1, 2 and 3 for different flow rates near the wall. These squares are representative of others levels (4, 5, 6 and 7, 8, 9).

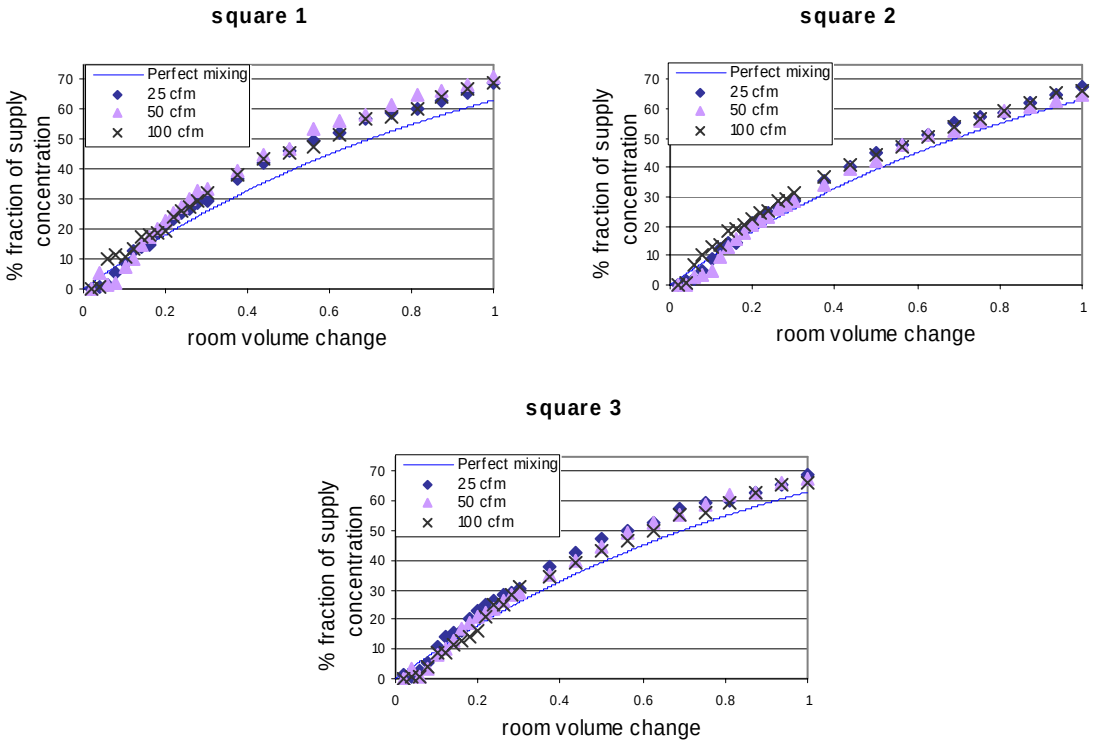

Figure 18: Cooling simulation, high inlet, near wall, squares 1, 2 and 3

The 25 cfm flow rate experiments were similar (concentrations are within 10% for a given room volume change) to the 100 cfm and 50 cfm flow rates, and, in general, concentrations near the wall were higher than those obtained at the centerline. The near wall time delays were longer than time delays at the centerline for the 25 cfm and 50 cfm flow rates. This is the opposite of the results for the ventilation system simulation because the negatively buoyant jet fell to the bottom of the tank and did not develop the same circulation pattern as for the ventilation case. For the 100 cfm flow rate the flow pattern was more like that of the ventilation case and there was less delay near the wall.

Table 4. Time delays near the wall for cooling simulations and a high inlet			
Square	Full scale time delay 25 cfm	Full scale time 50 cfm	Full scale time 100 cfm
1	1 min 8 sec	35 sec	No delay
2	58 sec	37 sec	No delay
3	26 sec	38 sec	26 sec
4	No delay	No delay	No delay
5	No delay	No delay	No delay
6	No delay	No delay	18 sec
7	No delay	No delay	No delay
8	No delay	No delay	9 sec
9	No delay	No delay	20 sec

Discussion of high inlet cooling results

For the specific locations within the room that we evaluated, the dye concentrations were uniformly greater than those for the perfect mixing case. This result occurs because the square locations we chose to study contained the supply jet and it's induced circulation pattern. We observed that other locations in each measured plane had lower concentrations. In the future, examining other planes within the tank could give more information on locations within the room where concentrations are lower than for the perfect mixing case. Another issue is that the water leaving the tank was not at the well-mixed concentration. In most cases the water leaving the tank had very little mixing with the rest of the tank and was at a high concentration as the jet flowed across the tank, impinged on the far wall, flowed down the wall and then exited through the outlet. For the cooling experiments, the effect was less pronounced than for the ventilation simulation because the jet fell down into the middle of the tank and produced a relatively well mixed zone below the stratification interface.

The stratification phenomenon with the 25 cfm and 50 cfm flow rates could be a source of discomfort. However, we calculated the worst temperature difference within the occupied zone to be about 1°C (for 0.06 room volume change and near the wall, square 1 had about 1% of fraction of supply and square 7 had 11% of fraction of supply concentration, which represented a 1°C temperature difference between the two squares). For this temperature difference, few occupants would express discomfort.

The time delays to reach each square were reasonably short (ranging from no measurable delay to about one minute) that any reasonable HVAC system cycle time (ten minutes or more) would ensure that conditioned air reached all the locations we examined.

In conclusion, we can say that this inlet-outlet configuration seems to be a good configuration to cool down a residential room and that flow rates of 25 cfm or higher should be sufficient to obtain reasonable mixing within the room.

Low inlet

The register location was changed to have the supply on the wall near the bottom of the tank, and the return at the top of the opposite wall. This configuration of a high return is not a usual register installation unless the system uses high mounted transfer grilles. The images can be inverted to represent a heating system with a high wall inlet and door undercut outlet.

As a result of laser system electronic problems, we were only able to perform experiments near the wall for this configuration. Figure 19 shows the strong stratification near the wall for this register configuration. The two lower flow rates had approximately the same flow patterns. The stratification interface was clearer for the 25 cfm flow rate. For the 100 cfm flow rate we observed more turbulence and the stratification interface was nearer the top of the room than for the other two flow rates.

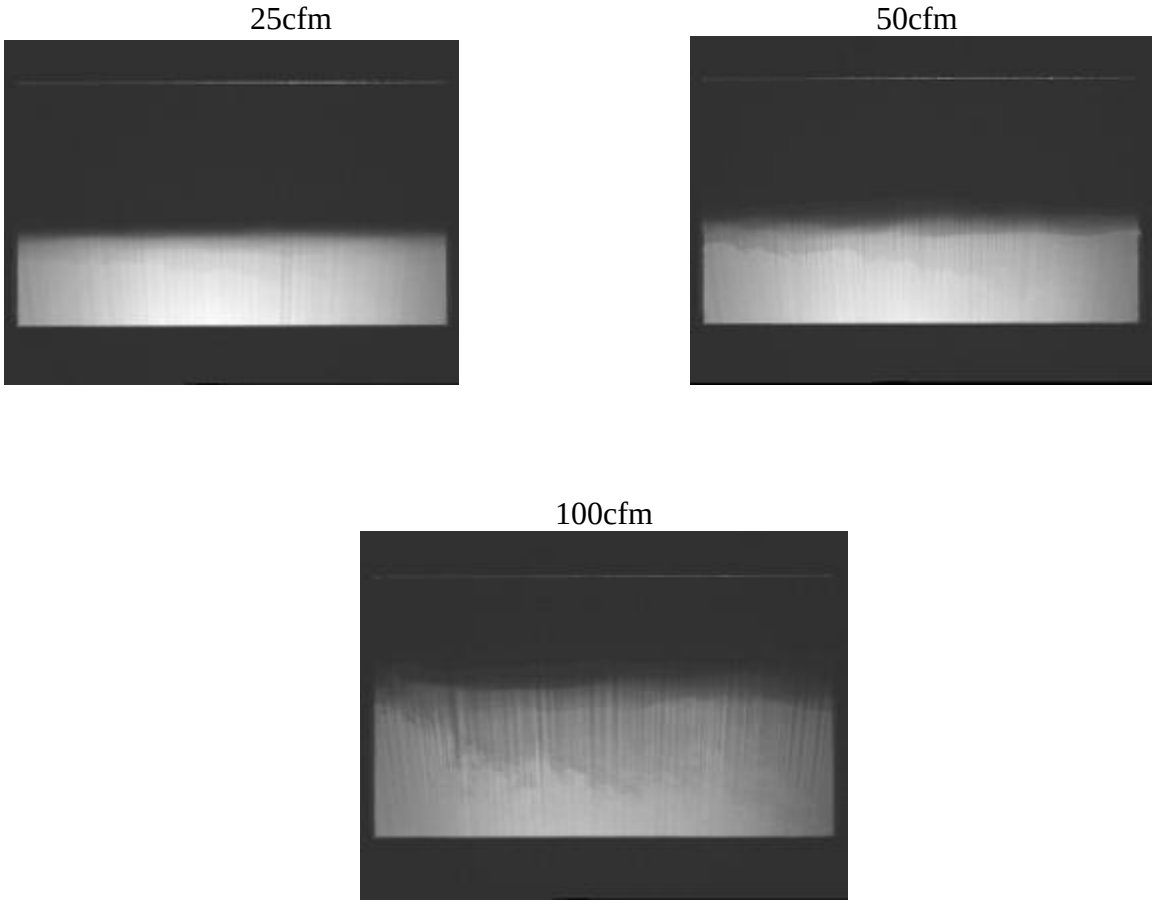

Figure 19. Cooling near wall example images for low inlet

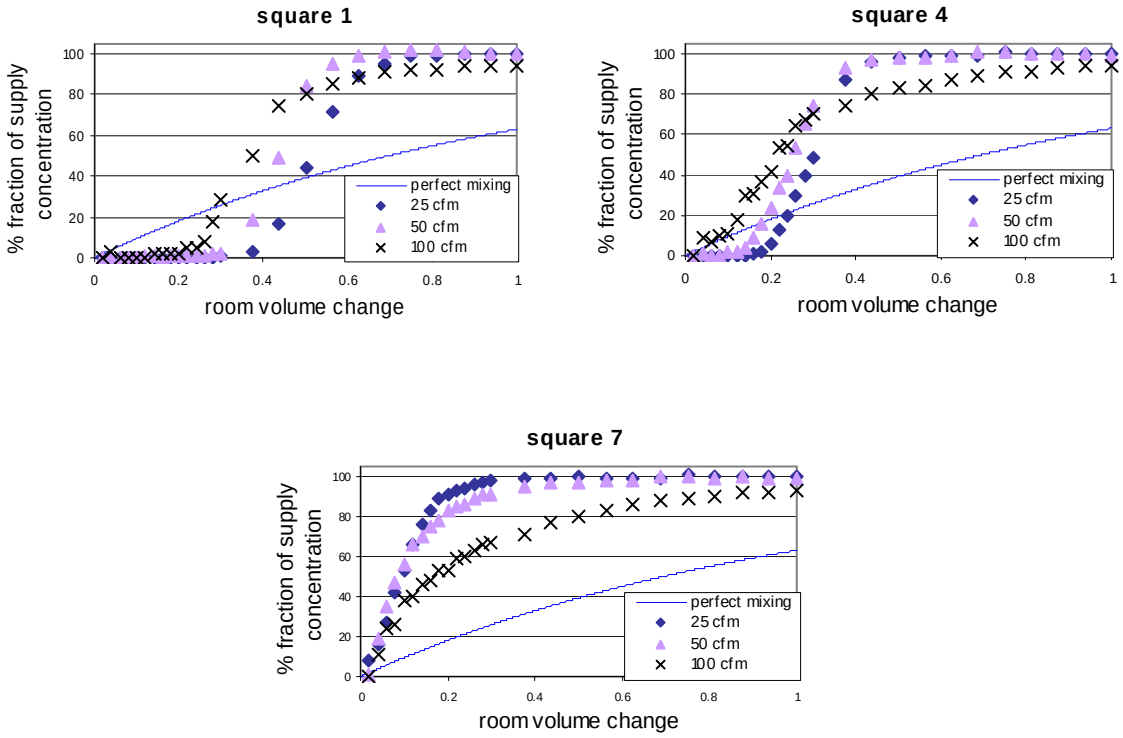

Figure 20: Cooling simulation, low inlet, near the wall, squares 1, 4 and 7

The results in Figure 20 are representative of other squares. The results in this configuration show complete stratification. 100% of fraction of supply concentration was reached in all cases after the stratification interface passed through the square being analyzed. The return water flow discharge did not contain dye until the dye level reached the outlet. Time delays (summarized in Table 5) were very long for the 25 cfm and 50 cfm flow rates due to the stratification. The 100 cfm flow rate had better results due to slightly improved mixing at this flow rate.

Table 5. Time delays near the wall for cooling simulations and a low inlet

Square	Full scale time delay 25 cfm	Full scale time 50 cfm	Full scale time 100 cfm
1	18 min 13 sec	7 min 53 sec	1 min 35 sec
2	18 min	7 min 21 sec	1 min 13 sec
3	17 min 50 sec	7 min 11 sec	1 min 13 sec
4	8 min 35 sec	2 min 17 sec	11 sec
5	8 min 13 sec	2 min 48 sec	21 sec
6	7 min 53 sec	2 min 48 sec	31 sec
7	31 sec	10 sec	10 sec
8	21 sec	No time delay	10 sec
9	No time delay	No time delay	No time delay

Discussion of low inlet cooling results

The combination of long time delays and the temperature gradients due to stratification mean that this register configuration should be avoided for cooling. As an example, for a 25 cfm flow rate at 0.15 room volume change, there was no supply air in squares 4, 5 and 6 and about 70% supply air in squares 7, 8 and 9. This translates to a 7°C air temperature difference between the head and ankles, which would result in local discomfort for about half of the occupants.

Heating system analysis

The heating system analyses were performed by inverting the images obtained with the high density supply as illustrated in Figure 21. The images then represent a heating system with a high wall supply and air leaving through a door undercut or low wall return.

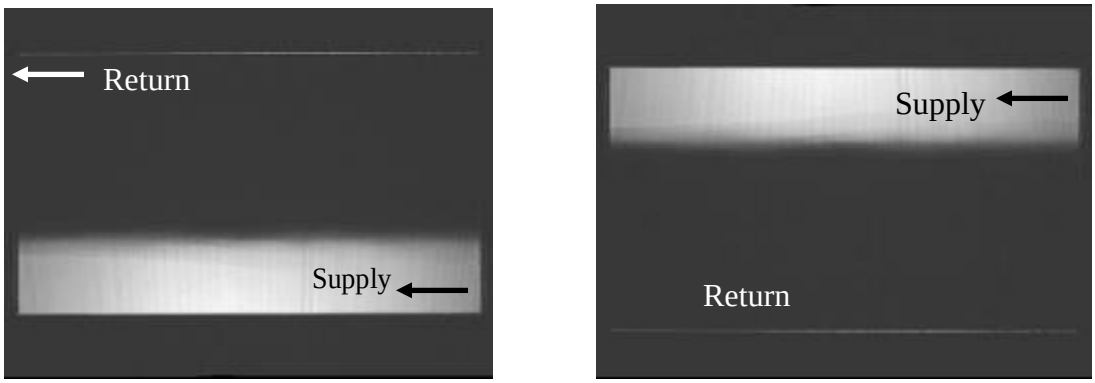

Original image Inverted image

Figure 21. Example Image Inversion for Heating Analysis

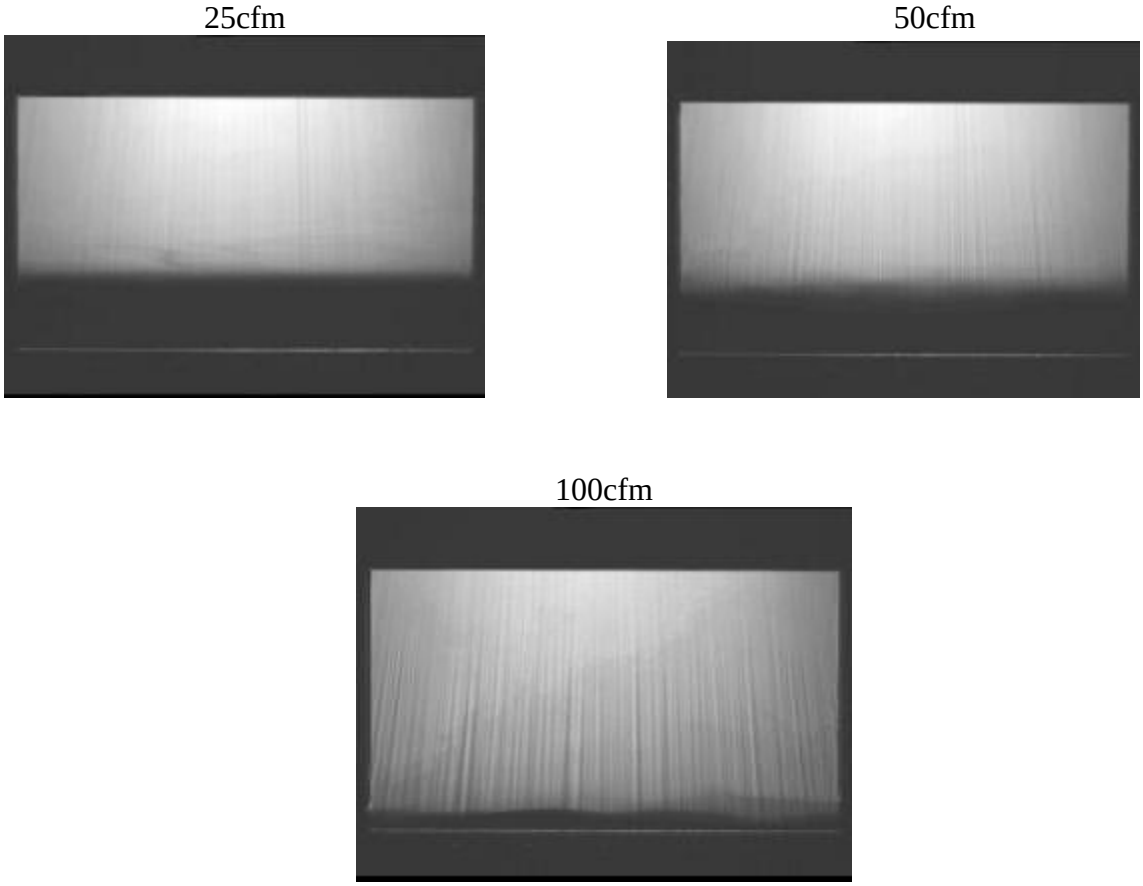

Figure 22. Comparison of stratification patterns near the wall for heating with high supply register and low return.

The images in Figure 22 illustrate the near wall concentrations after the same volume of air has been supplied (i.e., the time between system start up and when the image were taken is four times longer for 25 cfm compared to 100 cfm). Theses images show how the increased flow rates lead to a less sharp boundary between the stratification layers. Also, there is increased mixing as the flow rate is increased as indicated by the boundary extending further into the tank at the higher flow rates. The calculated concentration results in Figure 23 are slightly different from the cooling case discussed above due to a change in the location of the test measurement/analysis squares relative to the supply and return locations within the tank.

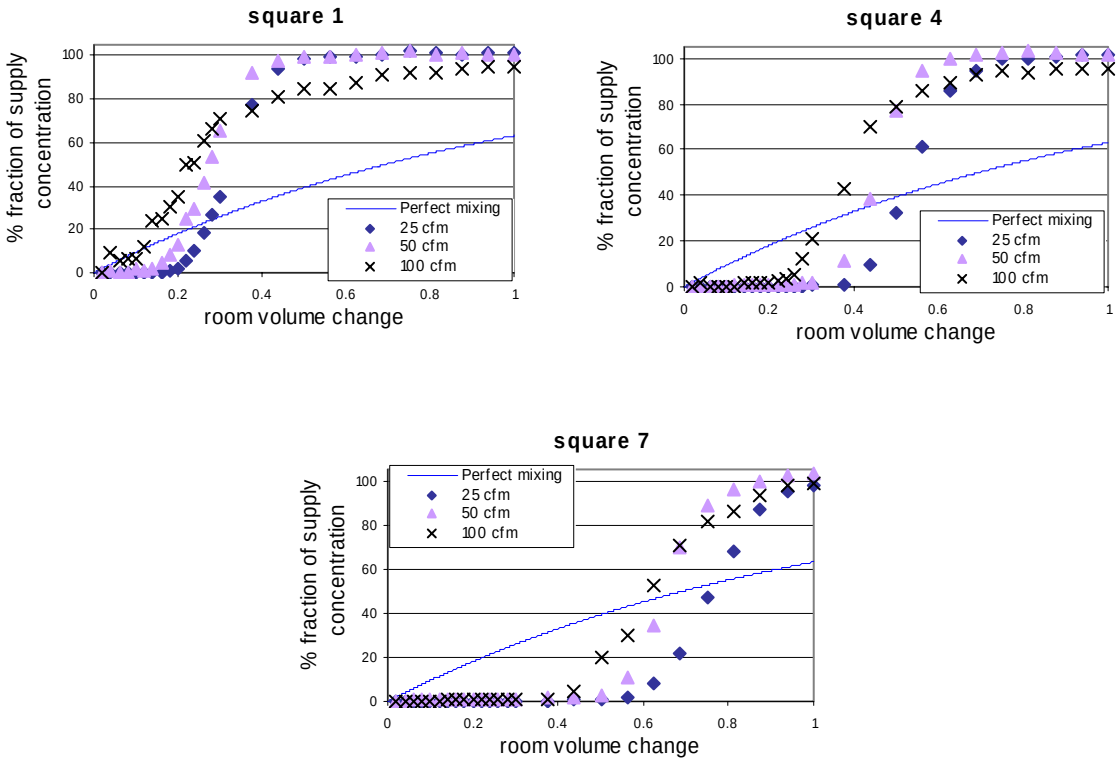

Figure 23: Heating simulation, inlet up, near the wall, squares 1, 4 and 7

The results shown in Figure 23 clearly show the stratification phenomenon. The concentration is essentially zero until the dye interface passes through the location being studied. It then rapidly increases to be the same as the concentration at the supply. The speed with which this takes place is an indication of how sharp the transition is at the interface. The results confirm the observations from Figure 22: as the flow rate increases, the transition becomes less sharp, and at 100 cfm the quasi-equilibrium concentration after the interface has passed the measurement location is less than 100% due to mixing elsewhere in the tank.

Table 6. Time delays near the wall for heating simulations and a low inlet

Square	Full scale time delay 25 cfm	Full scale time delay 50 cfm	Full scale time delay 100 cfm
1	10 min	4 min	21 sec
2	9 min 38 sec	3 min 40 sec	42 sec
3	9 min 48 sec	3 min 40 sec	42 sec
4	19 min 47 sec	8 min 45 sec	1 min 45 sec
5	19 min 16 sec	8 min 24 sec	2 min 48 sec
6	19 min 26 sec	8 min 14 sec	2 min 48 sec
7	29 min 36 sec	13 min	5 min
8	29 min	13 min 8 sec	4 min 44 sec
9	28 min 43 sec	11 min 44 sec	4 min 44 sec

Time delays were considerable for all the flow rates, and followed the usual pattern of being shortest for higher flows. The stratification phenomenon clearly contributes to these time delays. Almost a half an hour was required to reach squares at the bottom with the 25 cfm flow rate. In the best case, 5 minutes were required to reach those squares with the 100 cfm flow rate. Note that the time delays do not simply scale with the flow rate, i.e., the 25 cfm time delays are not four times those at 100 cfm. This is due to mixing effects and changes in jet trajectories for the different flow rates.

Discussion of low inlet cooling and high inlet heating simulations

Two significant issues were evident from those experiments. First, the time delays were too long, mostly because of stratification. For typical residential system cycle lengths of about ten to twenty minutes this register configuration does not get conditioned air to much of the conditioned space during system operation (after the system shuts down there may be some additional mixing). The stratification also led to significant temperature gradients in the occupied zone. As an example, for 25 cfm flow rate at 0.5625 room volume change, there was no supply air in squares 7, 8 and 9 and about 60 % supply concentration in squares 4, 5 and 6. This is equivalent to 6°C air temperature difference between the head and ankles for a seated person, which would result in discomfort for 40% of occupants.

Summary and Conclusions

Air flow patterns inside a room due to HVAC system operation were studied using a water-filled 1:10 scale model and a Planer Laser-Induced Fluorescence (PLIF) flow visualization system. Three supply register air flow rates of 25 cfm, 50 cfm and 100 cfm were examined so that we could observe differences between ventilation operation (at low flow rates) and heating or cooling operation (at higher flow rates), and the effects of operating multi-capacity systems in their lower capacity modes. The density differences between conditioned air and room air were simulated by increasing the density of the water in the experiments using salt. Heating system operation was derived by inverting the images obtained using the salt solutions. Two register placements were examined: high inlet/low outlet and low inlet/high outlet. The results were analyzed for comfort by looking at the spatial variation of thermal conditions inferred from the dye concentrations determined by the experiments, and comparing the spatial variation to acceptable limits. The time taken for certain conditions to be reached was analyzed by comparison to typical thermal HVAC cycle times and what reasonable expectations of performance might be for occupants.

High inlet/low outlet:
For ventilation this configuration gave good mixing. For cooling this configuration gave good thermal distribution for all flow rates. Also the time response was fast enough to be inconsequential for reasonable HVAC cycle lengths. For heating the results were more variable. At the high flow rate of 100 cfm, there was sufficient mixing that the time delay for seated occupants to receive warm air was less than five minutes. However, at only 25cfm flow, the time delay increased to almost half an hour for seated occupants. This is longer than is typical for residential heating systems (Walker and Modera 1998, Titus 2006) The second is that the air temperature gradients are significant and this translates into thermal discomfort for about half the occupants. Both of these effects are mostly due to the strong stratification effect.

Low Inlet/high outlet:
This configuration was only studied for cooling. As with the high inlet/low outlet case for heating, the strong stratification at all air flow rates led to excessive time delays and thermal gradients.

These results imply that register location has a stronger influence than air flow rate in determining acceptable room air mixing. Therefore, the HVAC system designers concerns should be focused on the register locations rather than ensuring high register exit velocities.

Appendix 1: Test apparatus details

The test apparatus consists of several components:

- the scale model,
- the stand,
- the pump and piping for the supply water,
- the laser and cooling water circuit,
- the optics to spread the laser beam
- the CCD video camera and the video capture board to capture the images during the experiments.

The following picture shows the test apparatus as it was used for the experiments.

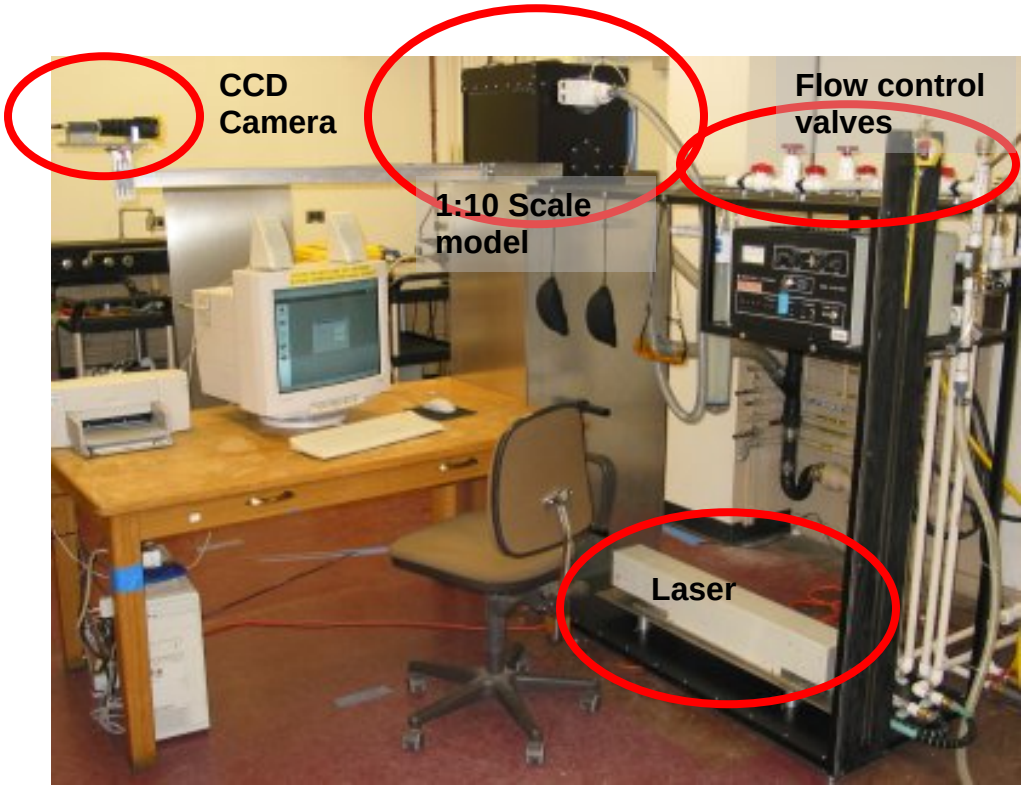

Figure 1.1. Test Apparatus

For our experiments we used a 1:10 scale model of a 14'x 12' x 8' room. Using a room of this size better represents a typical residential room than the minimum room size of 24' x 18' x 9' specified by ASHRAE Standard 70, (ASHRAE 1991) for performance testing. The room has a centered 10" x 6" high sidewall air inlet 5.6" below the ceiling. In the wall opposite the inlet is a centered 31.12" x 1.88" door undercut serving as the return outlet. This setup represents a commonly used arrangement in houses.

Instead of a register or diffuser we just have a plain opening in the scale model, as it would be very difficult to built a 1:10 scale model of a register that can withstand the

pressure of the supply water. There are various types of high-end registers that aid the mixing process by generating turbulence and directing the airflow. But these registers are mostly used in commercial buildings while registers normally used in residential buildings are very inexpensive.

The scale model has a single clear face on the long side for observation of the flow pattern. The bottom has two slots with glass inserts where the vertical planes of laser light enter the test chamber. One slot is in the centerline and the other one is 1.2" from the front face. To drain the model after an experiment it has a sink drain in the bottom. During testing the drain is covered by a plug to create a level surface.

The top has a removable lid for quick draining and flushing. The top seal is placed some distance down the sidewalls so at the start of the experiment the tank can be slightly overfilled to aid in flushing out bubbles. The bubbles create problems because they become areas of bright light in the recorded images that complicate the image analysis. The supply opening is shut off with a ball valve as this kind of valve can be opened completely very quickly.

Figure1.2 Front view of the scale model

The stand was designed to be wide enough to allow the tank to slide to two different positions, so the experiments for the center plane as well as for the near-wall plane can be carried out without having to re-adjust the laser beam and the optics. The optics are mounted to the stand by a mechanism that allows the adjustment of the distance between the lenses as well as their vertical and lateral alignment.

The flow rate was set with a gate valve and the flow turned on and off using the separate ball valve. A separate branch with is own valves was used for each of the three flow rates. This made the flows much more repeatable because the valve that set the flows was not reset for each experiment. The water containing the dye was stored in a 100 L barrel and pumped from there into the tank using a submersible sump pump.

Figure 1.3 Flow control manifold

The flow rates were measured using a Gerand Venturi-nozzle ¾”-414 and a u-pipe-manometer. The change of static pressure across the nozzle was read directly off the u-pipe manometer. With this value the flow rate could be calculated from a calibration equation for the manometer.

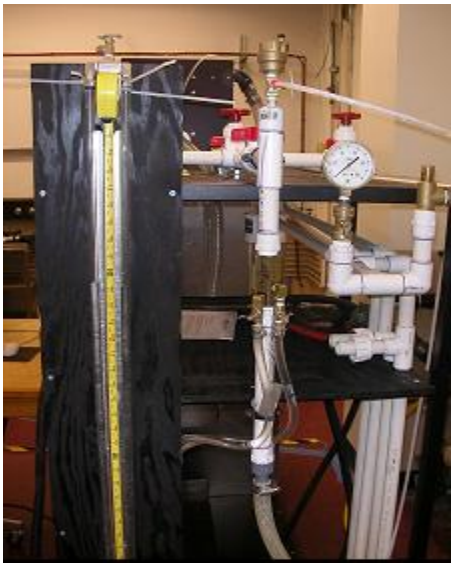

Figure1.4 Manometer and Venturi nozzle

A Spectra Physics model 168 class IV argon ion laser was used to generate the laser light sheets. The laser head and the power supply are mounted on the test stand. The laser head can be moved laterally and vertically to adjust the laser beam. The power supply and laser head were connected to a water-cooling circuit. A filter guarantees that the heat exchanger of the power supply does not clog during the experiments. A manometer and a safety relief valve were included in the cooling water circuit at the entry of the power supply to avoid damage by excessive water pressure.

Figure 1.5: The power supply

Figure 1.6: The laser head

Two cylindrical lenses were used to spread the laser beam and create the laser light sheets. The lenses are mounted to the stand by a mechanism that allows adjusting the distance between the lenses as well as their vertical and lateral alignment.

Figure 1.7: Cylindrical lenses and lens mounts

A monochrome Hitachi KP-M1 8 bit CCD camera with analog composite NTSC output was used to measure the fluorescence emitted from the laser-illuminated plane during the experiments. A selective light Kodak Wratten Filter # 15 was attached to the camera to prevent scattered laser light from reaching the camera. A camera mount that allowed three-dimensional adjustment of the camera's field of vision was built out of aluminum and connected directly to the tank. The images from the camera were digitized using a personal computer connected to an NTSC composite video capture board (Grabit Pro, Aims Laboratory). The digitized images provided a gray-level resolution of 256 values (i.e. 8-bit).

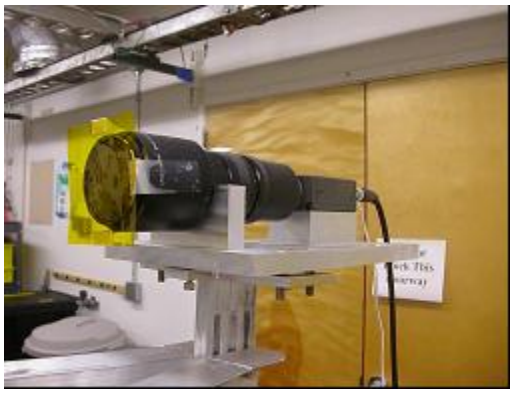

Figure 1.8: CCD Camera and filter

Appendix 2: Step by step experiment procedure

Preparing the dye solution

1. Weigh 80 mg of dye with a high-precision scale (Mettler AE 240, precision 0.0001g)
2. Mix the dye in a 1-liter volumetric flask to get the 0.08 g per liter dye solution.

Mixing the dye solution and preparing the tank

1. Mix the dye solution that will be pumped in the tank. The barrels have a 100L mark on the top of the rim. This 100 L mark was determined by pouring 100 one liter volumetric flaks of water into the barrel. Fill the barrel to this mark with fresh water and add 101 ml of the solution with a concentration of 0.08g of dye per liter.
2. If this is a heating or cooling experiment, add the salt before filling the barrel with fresh water to the 100L mark and mix the salt thoroughly with the water. Check the density with the hydrometer.
3. When running the test for the first time or after a long break the air bubbles must be purged from the piping. Open all three ball valves of the manifold and turn on the pump to flush out the bubbles.
4. Set the flow rate desired. Looking in the direction of flow, the left branch of the manifold should be adjusted to a flow rate of 1.167 gallons per minute (equivalent to 25 cfm air flow rate in full scale), the middle one to 2.334 gpm (50 cfm), and the right one to 4.668 gpm (100 cfm).
5. Rinse the tank thoroughly and then fill with fresh water. Use a squeegee to wipe off the air bubbles sticking to the bottom, walls, and ceiling of the tank. Open the bleeder valve on the slide valve the close the lid of the tank. Close the bleeder valve.

Preparing the image capturing

Open the Grabit Pro program. Choose sequence capture. Enter the setup.

1. Under General select 256 colors (8-bit). For the file format choose bitmap (bmp). At a resolution of 320 x 240 pixels the camera can take 1.68 pictures per second. At higher resolutions the rate is slower.

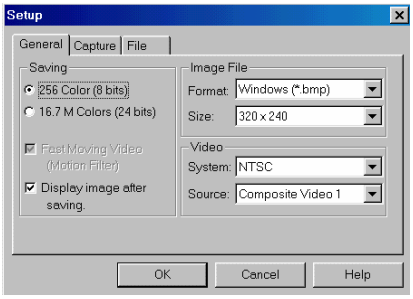

2. Under Capture choose normal capture mode. When fast capture mode is chosen only a limited amount of pictures can be taken. Enter the number of images you want to take. Even if the capture interval is set to 1 second image taking is slower.

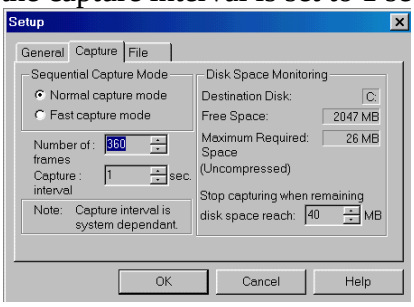

3. Under File you can choose a file name or code, e.g. 25cfm. Under Save as you can choose the folder you want to save the pictures in. You can also choose the next image count, normally 1. After each experiment you have to reset this field. Unfortunately Grabit Pro does not list the images in a numerical order. Image number 10 will appear after image number 1 instead after image number 9.

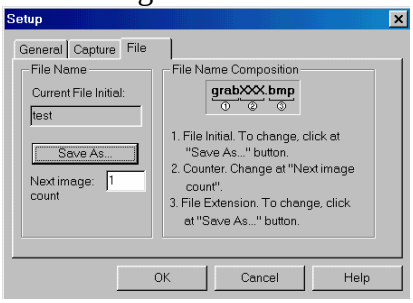

Starting the laser

1. Although the test stand is covered to shield reflected laser light you should always wear safety goggles before turning on the laser.
2. Open the cooling water circuit. Open the return valve first then open the supply valve very slowly to avoid overpressure. Otherwise the safety valve will open for a short moment.
3. Before turning on the power supply you have to check the settings. Make sure the control mode switch is set to current control. Never set it to light or field, as this will wear out the cathode in the laser head prematurely. Turn the meter dial to 50 Amps. Set the current control to zero. To switch on the power supply turn the key of the master control to on. Then turn the switch in the bottom left corner. When the ready light begins to glow you can start the laser. Let the cathode warm up for 10 seconds. Then turn up the power to 30 Amps on the current control.

Starting the experiment

1. Turn on the pump.
2. Turn off the laboratory lights. It is important that no light other than emitted from the dye reaches the camera.

3. Then open the slide valve and start the image capturing simultaneously.
4. During the experiment check that the flow rate is correct: Measure the distance between the water levels of the u-pipe manometer. The distance must be:

    - 2.8” for 1.167 gpm (≙ 25cfm air flow rate)
    - 11.2” for 2.344 gpm (≙ 50cfm air flow rate)
    - 45.0” for 4.668 gpm (≙ 100cfm air flow rate)

Completing the experiment

1. After the image capturing has completed turn off the pump.
2. Turn down the power to 10 Amps on the current control then turn off the bottom left corner switch and turn the key of the master control to off.
3. Turn on the laboratory lights and close the cooling system. Close the supply valve first then the return valve.

Appendix 3: Experiment image analysis

A computer program developed by one of the authors (Smith), written in the "C" computer language was used to analyze experiment images. All variables describing the geometry were entered in an input file. The results were recorded in an output file in comma separated value (csv) form that can be easily imported by Excel. The images to be analyzed must be in the same folder as the input file.

Required data are:

- Output file name

0% calibration picture filename
100 % calibration picture filename
First experiment picture filename
W, x1, x2, x3, y1, y2, y3, y4, measures marks shown as follows:

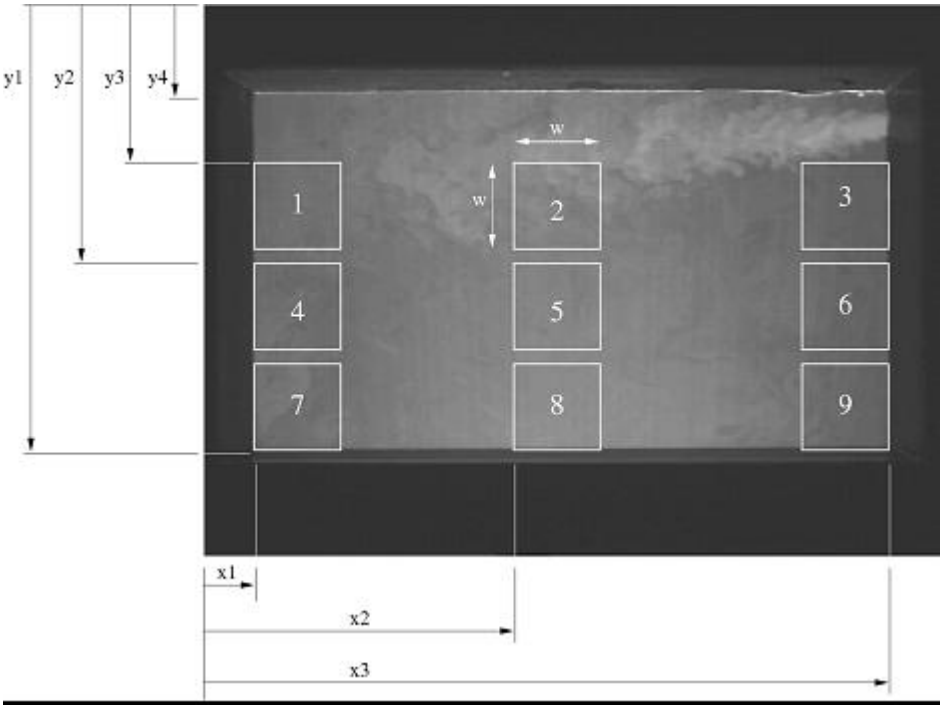

Figure 4.1 Analysis area/square locations

For centerline pictures in ventilation and cooling simulations:

W	X1	X2	X3	Y1	Y2	Y3	Y4
30	21	143	295	192	124	85	38

For wall pictures in ventilation and cooling simulations:

W	X1	X2	X3	Y1	Y2	Y3	Y4
33	11	142	307	197	122	80	29

For wall pictures in heating simulations:

W	X1	X2	X3	Y1	Y2	Y3	Y4
33	11	143	307	209	134	92	41

The a and b calibration equation parameters ($y= ax^2+bx$, where y is the fraction of supply concentration and x is the measured intensity).
Y or n, to choose if resultant images should be created. These include the calibration image after subtracting the baseline image and other images for diagnostic purposes.

Program description:

1. The image taken with fresh water only (the baseline image) is subtracted from each experiment image.
2. The baseline picture is subtracted from the 100 % calibration picture.
3. Then experiments pictures are divided by the new calibration picture and multiplied by the mean intensity of this calibration picture.
4. The mean intensity value and the standard deviation are measured in each square.
5. The calibration equation is used to determinate the % fraction of supply concentration.
6. If “y” is chosen for the “output image” flag, the program creates the results pictures in the same folder as the experiment pictures.

The results are recorded in a comma separated values (csv) file.

Appendix 4: Perfect mixing concentration estimates

In this case, the dye added to the tank is immediately and perfectly mixed with the water in the tank. The dye concentration is consistent throughout the tank.
Therefore, the dye concentration within the tank and the dye concentration leaving the tank are the same.

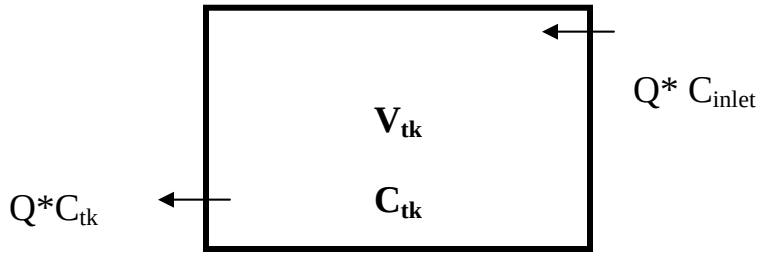

With Q: Flow rate (m^3 per sec)
Vtk: Tank Volume (m^3)
Ctk: Tank dye concentration (%)
Cinlet: Inlet dye concentration = 100 %
$C^1_{tk}(t)$: Time differential for Tank dye concentration

Governing equations:

$$\frac{d\,(Vt_k * C_{tk})}{dt} = Q * (C_{inlet} - C_{tk}) \quad (5.1)$$

$$V_{tk} * C^1_{tk}(t) = Q * C_{inlet} - Q * C_{tk}(t) \quad (5.2)$$

$$C^1_{tk}(t) + \frac{Q}{V_{tk}} * C_{tk}(t) = C_{inlet} * \frac{Q}{V_{tk}} \quad (5.3)$$

However:

$$\frac{Q}{V_{tk}} = \frac{1}{To} \quad (5.4)$$

Where, To is the time for one tank volume change.
So

$$C^1_{tk}(t) + \frac{C_{tk}(t)}{To} = \frac{C_{inlet}}{To} \quad (5.5)$$

The solution of this equation is:

$$C_{tk}(t) = C_{inlet} * (1 - \exp(-\frac{t}{To})) \quad (5.6)$$

So for each flow rate, the concentration within the tank is function of time.
Value of To:

Flow rate in the full scale	Time in the tank scale = To
25 cfm	518 sec
50 cfm	259 sec
100 cfm	129.5 sec

The perfect mixing curve was plotted as a function of the room volume change. Since we know that To is the time for one volume change, it is easy to determine the relationship between the tank dye concentration and the volume change.

$$Q = \frac{V_{tk}}{To} \quad and \quad Q = \frac{V}{t} \tag{5.7}$$

So

$$\frac{t}{To} = \frac{V}{V_{tk}} \tag{5.8}$$

So for all flow rates there is a unique perfect mixing curve as a function of the room volume change.

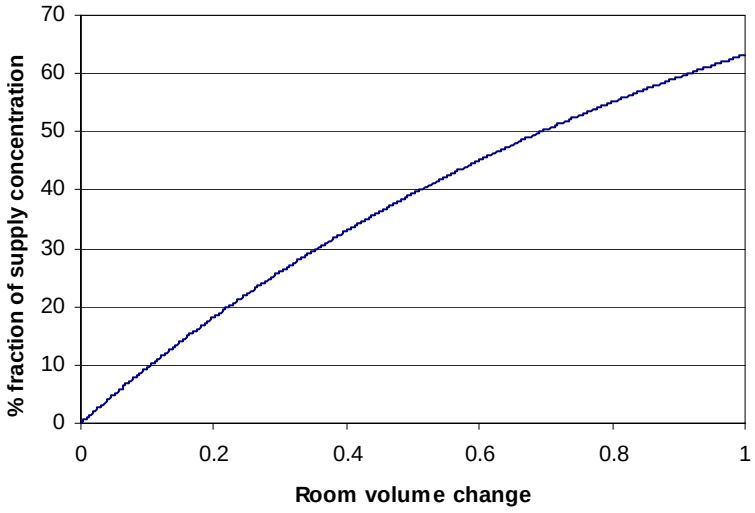

Figure 5.1 Perfect mixing curve

Appendix 5: Time delay calculations

Time delays were calculated compared to the perfect mixing equation.
The perfect mixing equation was:

$$C_{tk}(t) = C_{inlet} * (1 - \exp(-\frac{t}{To}))$$

As we knew that the real case couldn't be a perfect case, two parameters were introduced in the equation to determine an equation approaching the real results.
The two parameters were b and toffset.
So the experiment equation was:

$$C_{tk}(t) = C_{inlet} * (1 - \exp(-b(\frac{t - toffset}{To - toffset})))$$

A computer program called 'vin' was used to determine the two parameters toffset and b for each square and each flow from experimental points.
Data were entered into Stata from an input csv file (% fraction of supply concentration as a function of time). The result was the curve drawn and the two parameters with their confidence intervals ($B0=b$ and $B1= t_{offset}$) as shown below.

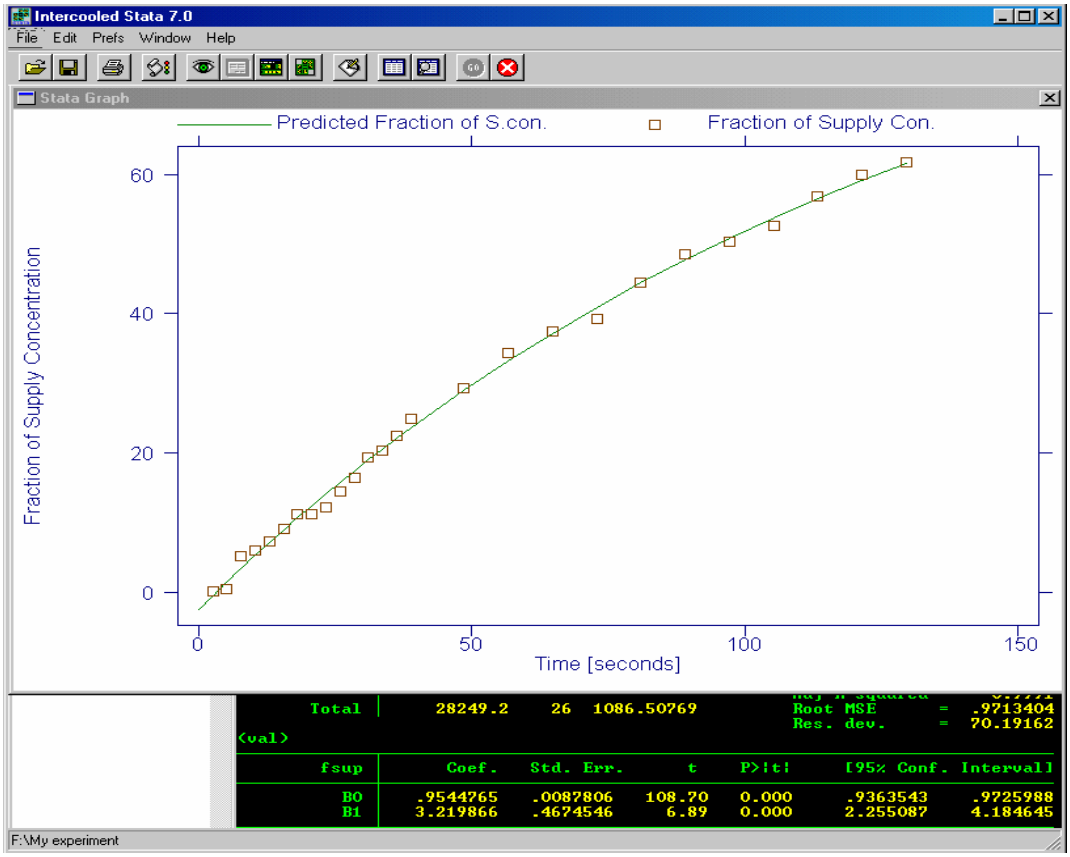

Figure 6.1 : Intercooled Stata Version 7 example time evolution of concentration analysis to find time offset

Interpretation of b and toffset results:

b is always positive and if its value is close to 1.00 it means that the data points follow the same progression as that of the perfect mixing case.
t_{offset} can be either positive or negative. A positive value has a physical significance. It is the time delay before any dye is seen in the area, which corresponds to the time taken for the flow to travel from the register to the sample area.
A negative value has no physical meaning because it is obvious that no dye could be in the square before the experiment had begun. So a negative toffset means that the dye concentration in the square studied at the instant t= 0 + ε, where ε is a very short time, is higher than the dye concentration in the same square at the same moment for the perfect mixing case.
For example, squares that are in the jet direction, receive more dye than in the perfect mixing case.

Appendix 6: Experimental Results

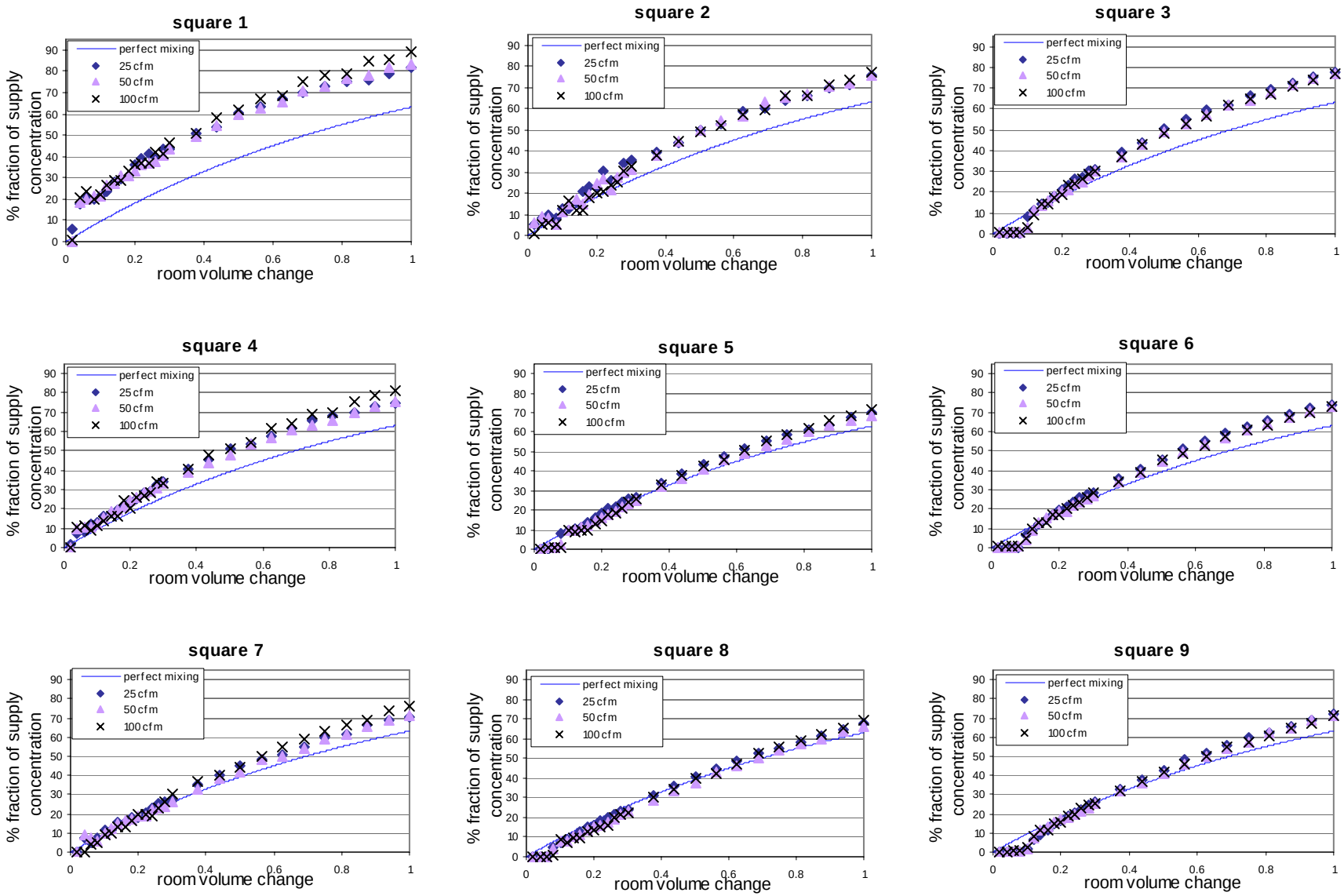

Figure 7.1: ventilation simulation, inlet up-outlet down, centerline, squares 1-9

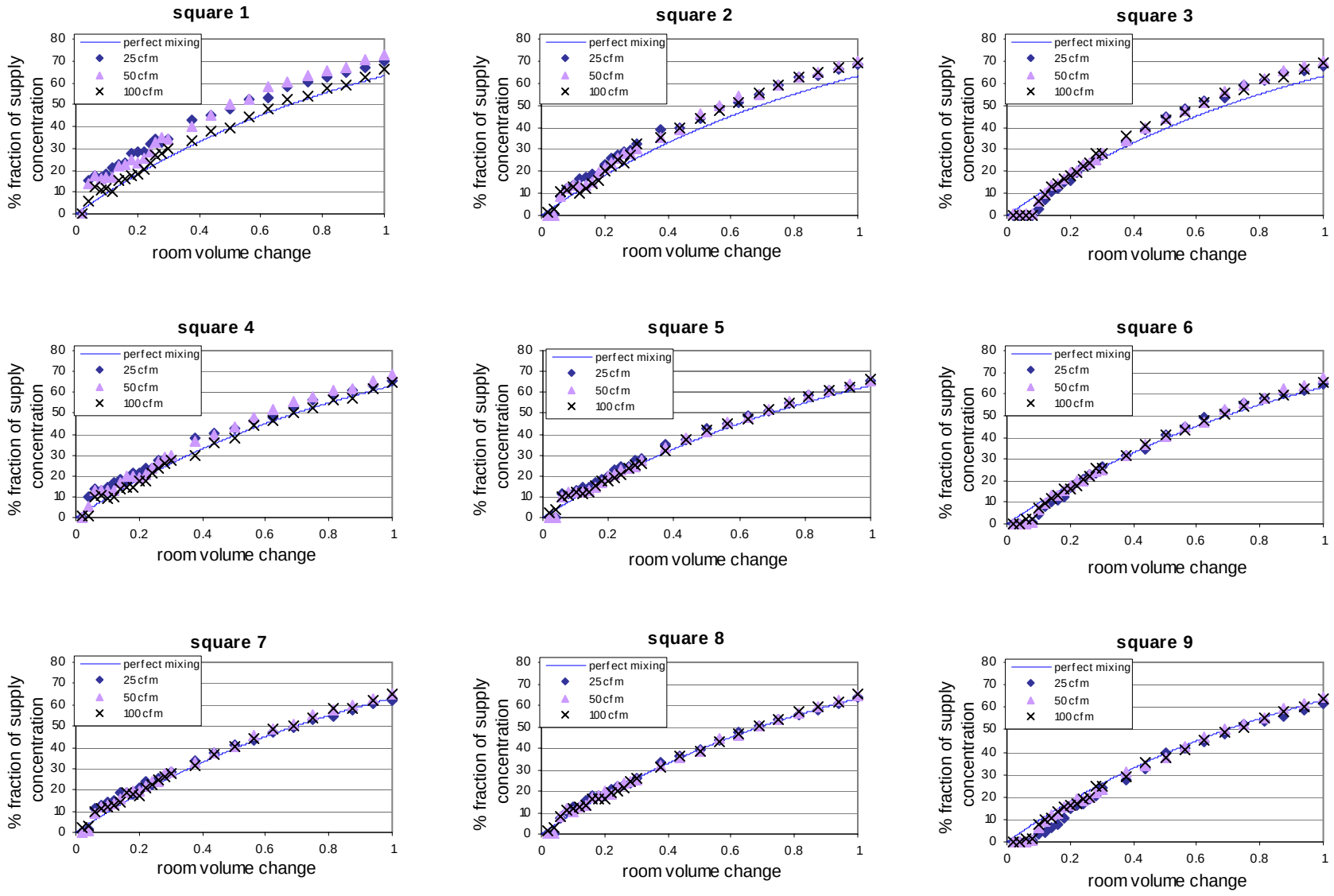

Figure 7.2: ventilation simulation, inlet up-outlet down, near the wall, squares 1-9

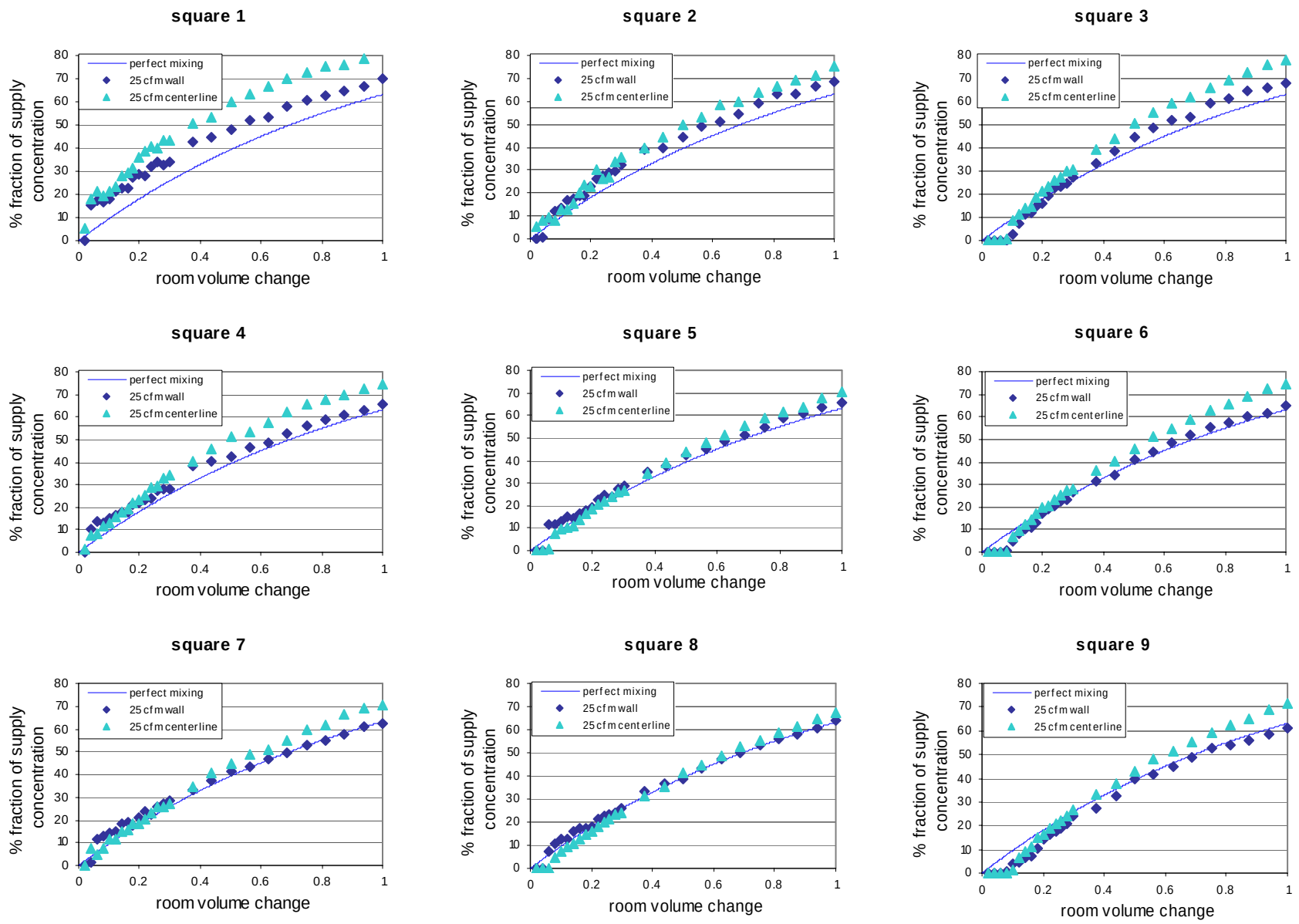

Figure 7.3: Ventilation simulation, inlet up-outlet down, comparison between centerline and near the wall, 25 cfm, squares 1-9

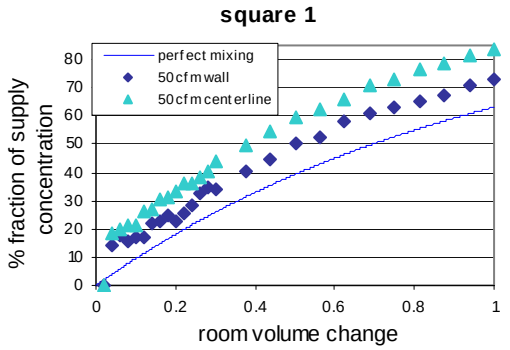
square 1
perfect mixing
50 cfm wall
50 cfm centerline
% fraction of supply concentration
room volume change
0
10
20
30
40
50
60
70
80
0
0.2
0.4
0.6
0.8
1

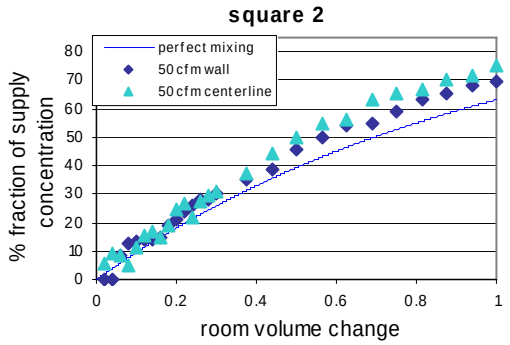
square 2
perfect mixing
50 cfm wall
50 cfm centerline
% fraction of supply concentration
room volume change
0
10
20
30
40
50
60
70
80
0
0.2
0.4
0.6
0.8
1

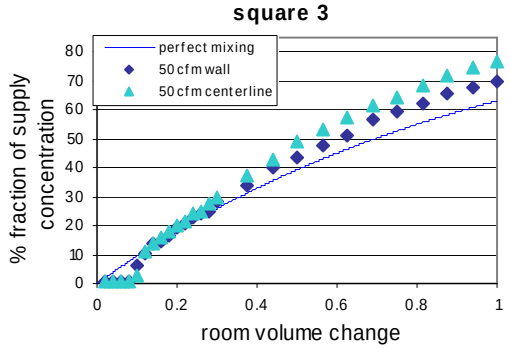
square 3
perfect mixing
50 cfm wall
50 cfm centerline
% fraction of supply concentration
room volume change
0
10
20
30
40
50
60
70
80
0
0.2
0.4
0.6
0.8
1

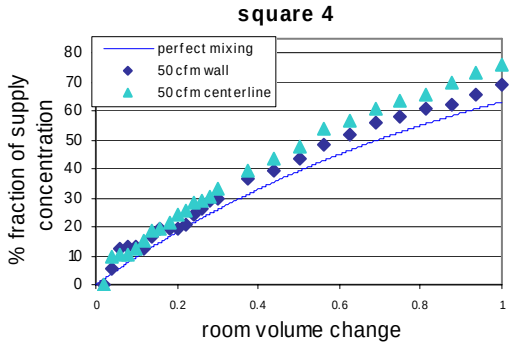
square 4
perfect mixing
50 cfm wall
50 cfm centerline
% fraction of supply concentration
room volume change
0
10
20
30
40
50
60
70
80
0
0.2
0.4
0.6
0.8
1

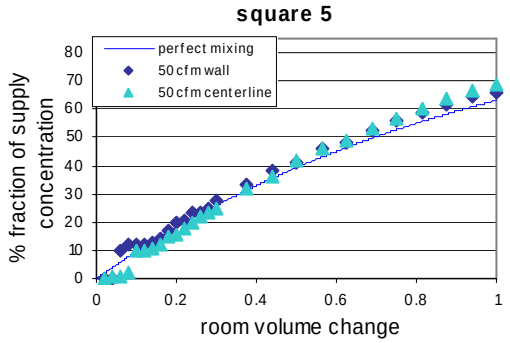
square 5
perfect mixing
50 cfm wall
50 cfm centerline
% fraction of supply concentration
room volume change
0
10
20
30
40
50
60
70
80
0
0.2
0.4
0.6
0.8
1

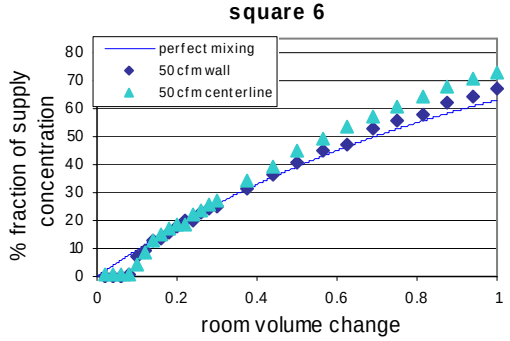
square 6
perfect mixing
50 cfm wall
50 cfm centerline
% fraction of supply concentration
room volume change
0
10
20
30
40
50
60
70
80
0
0.2
0.4
0.6
0.8
1

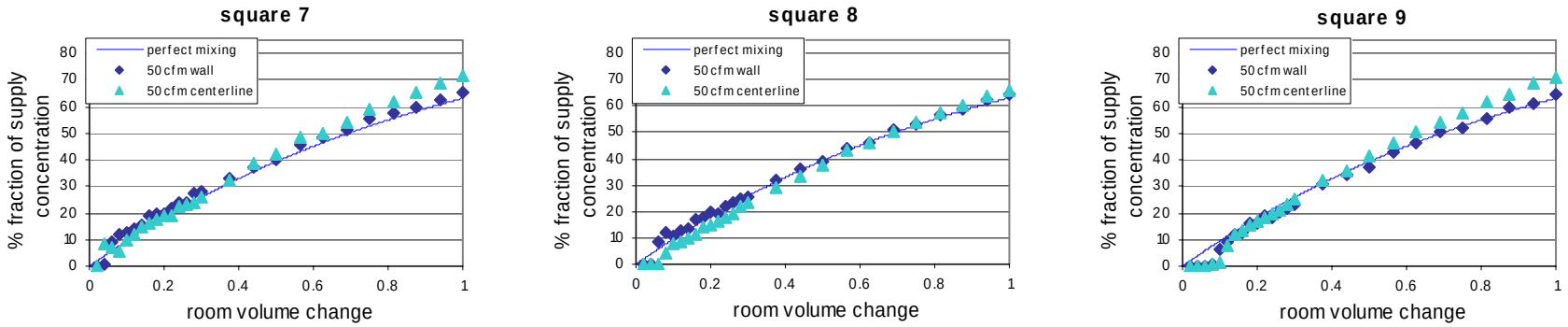

Figure 7.4: Ventilation simulation, inlet up-outlet down, comparison between centerline and near the wall, 50 cfm, squares 1-9

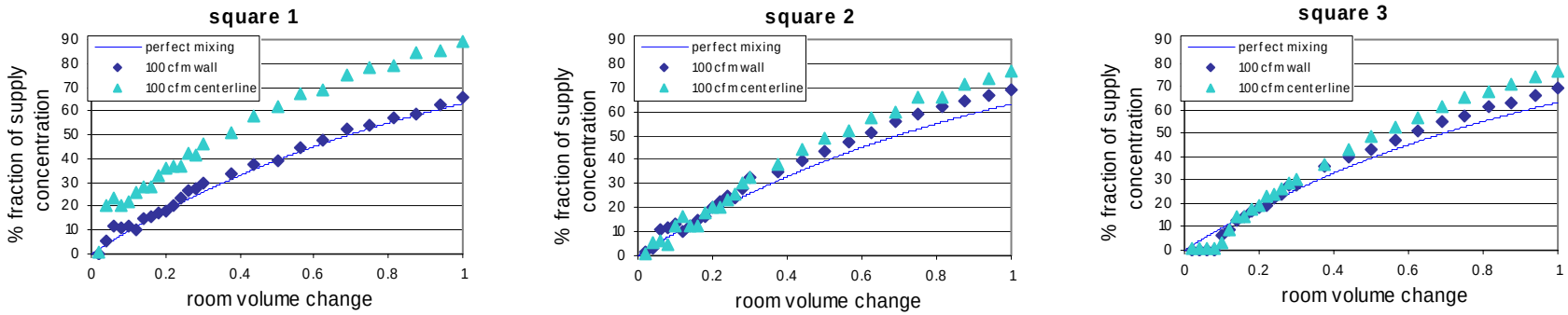

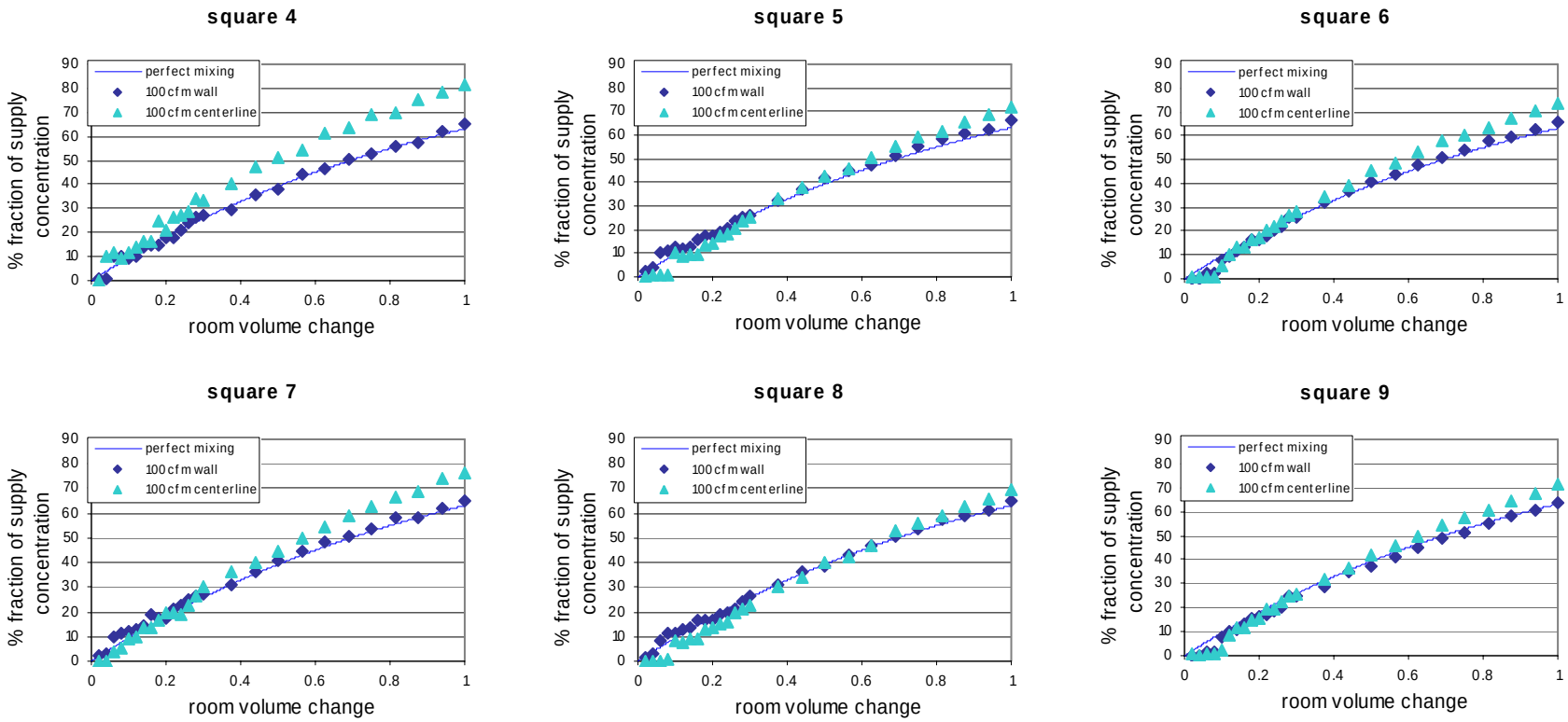

Figure 7.5: Ventilation simulation, inlet up-outlet down, comparison between centerline and near the wall, 100 cfm, squares 1-9

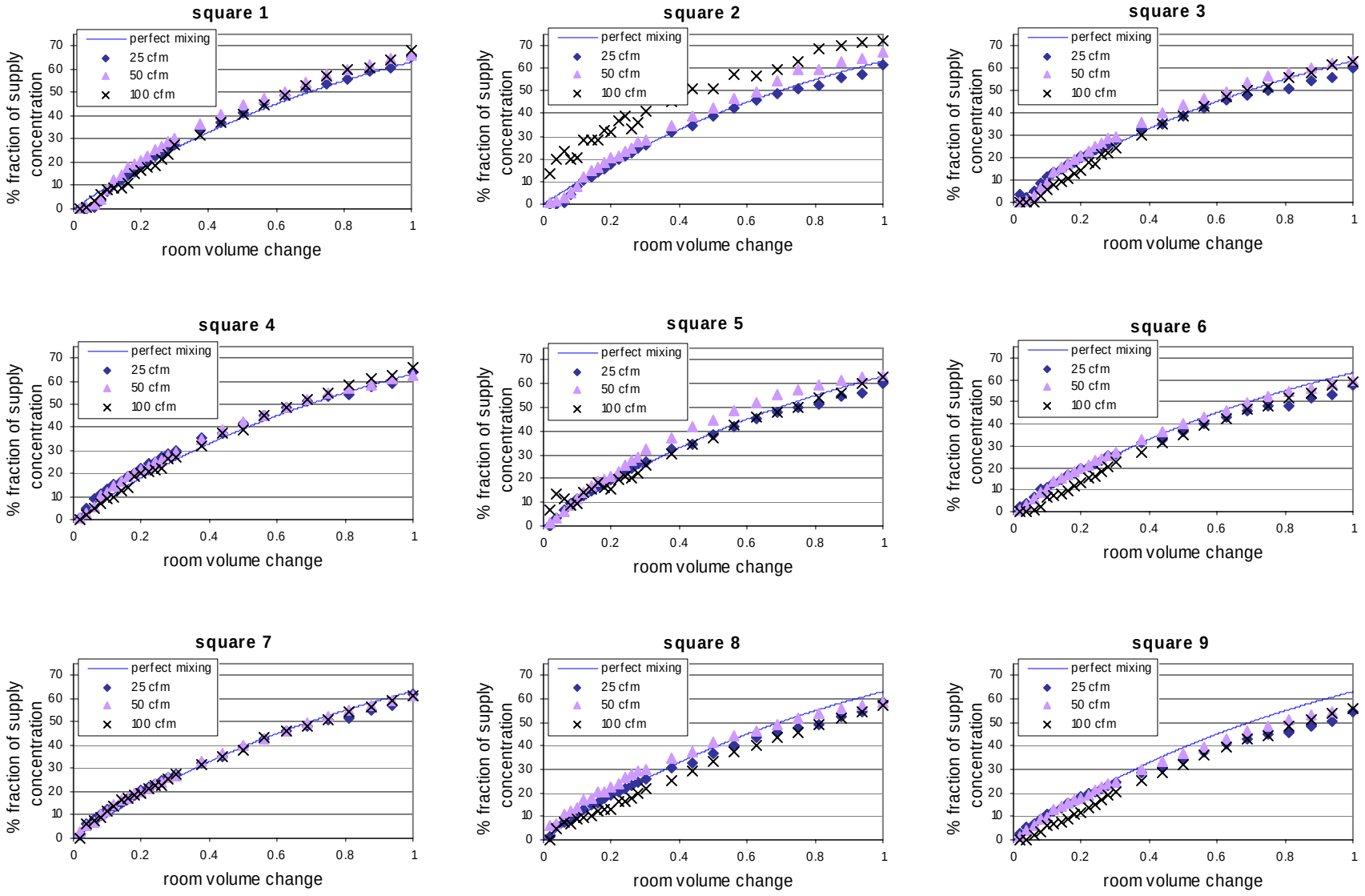

Figure 7.6: Cooling simulation, inlet up-outlet down, centerline, squares 1-9

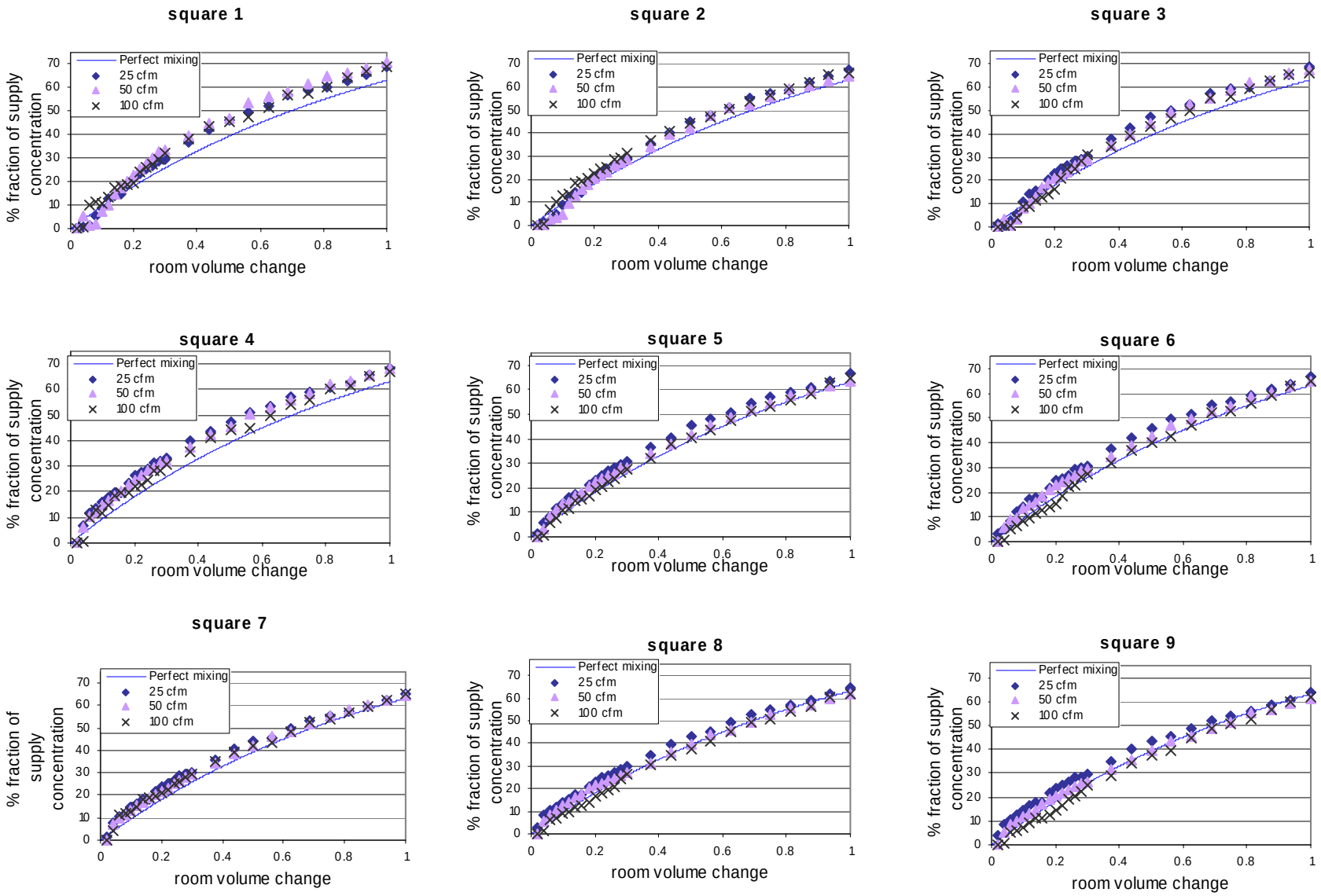

Figure 7.7: Cooling simulation, inlet up-outlet down, near the wall, squares 1-9

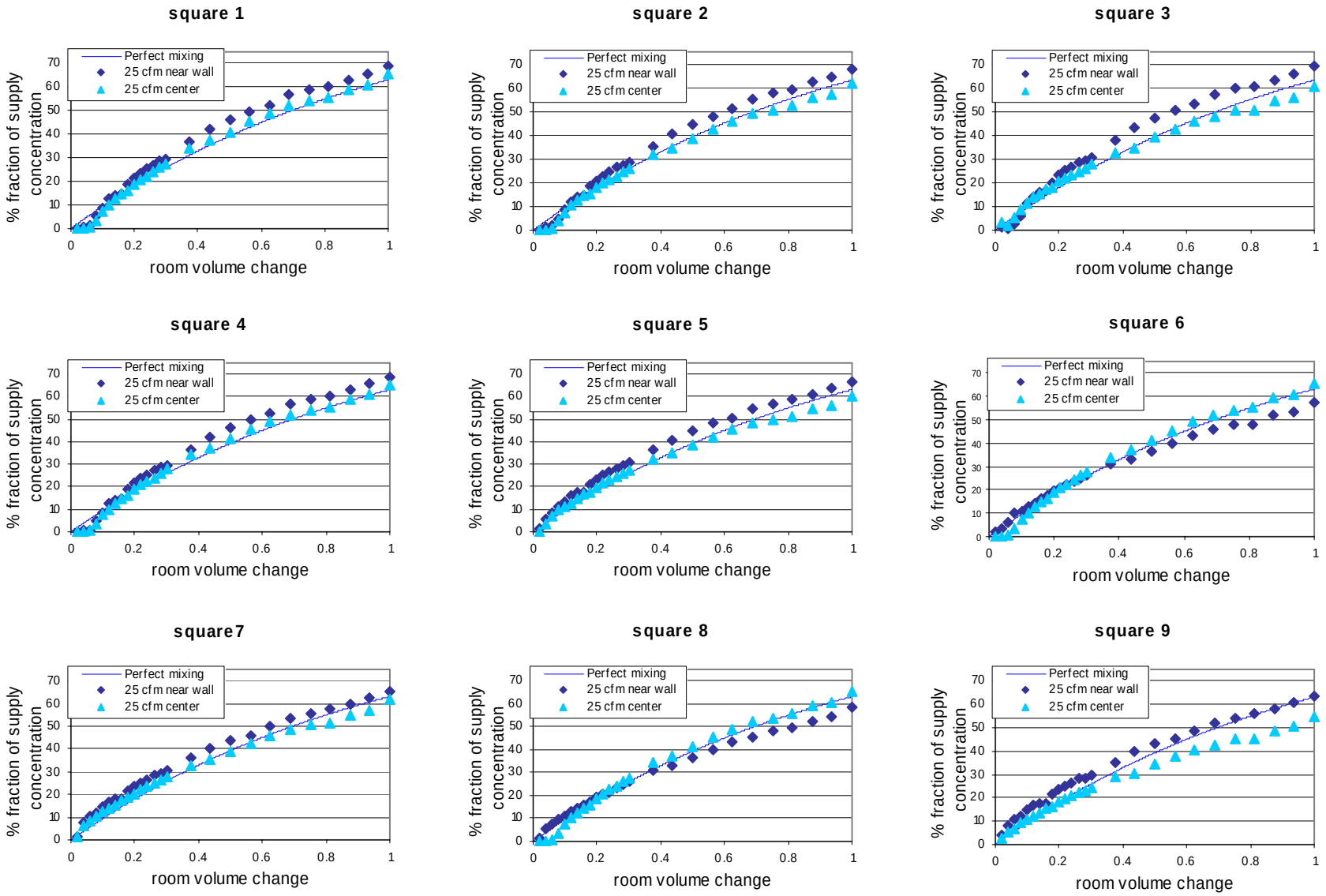

Figure 7.8: Cooling simulation, inlet up-outlet down, comparison between centerline and near the wall, 25 cfm, squares 1-9

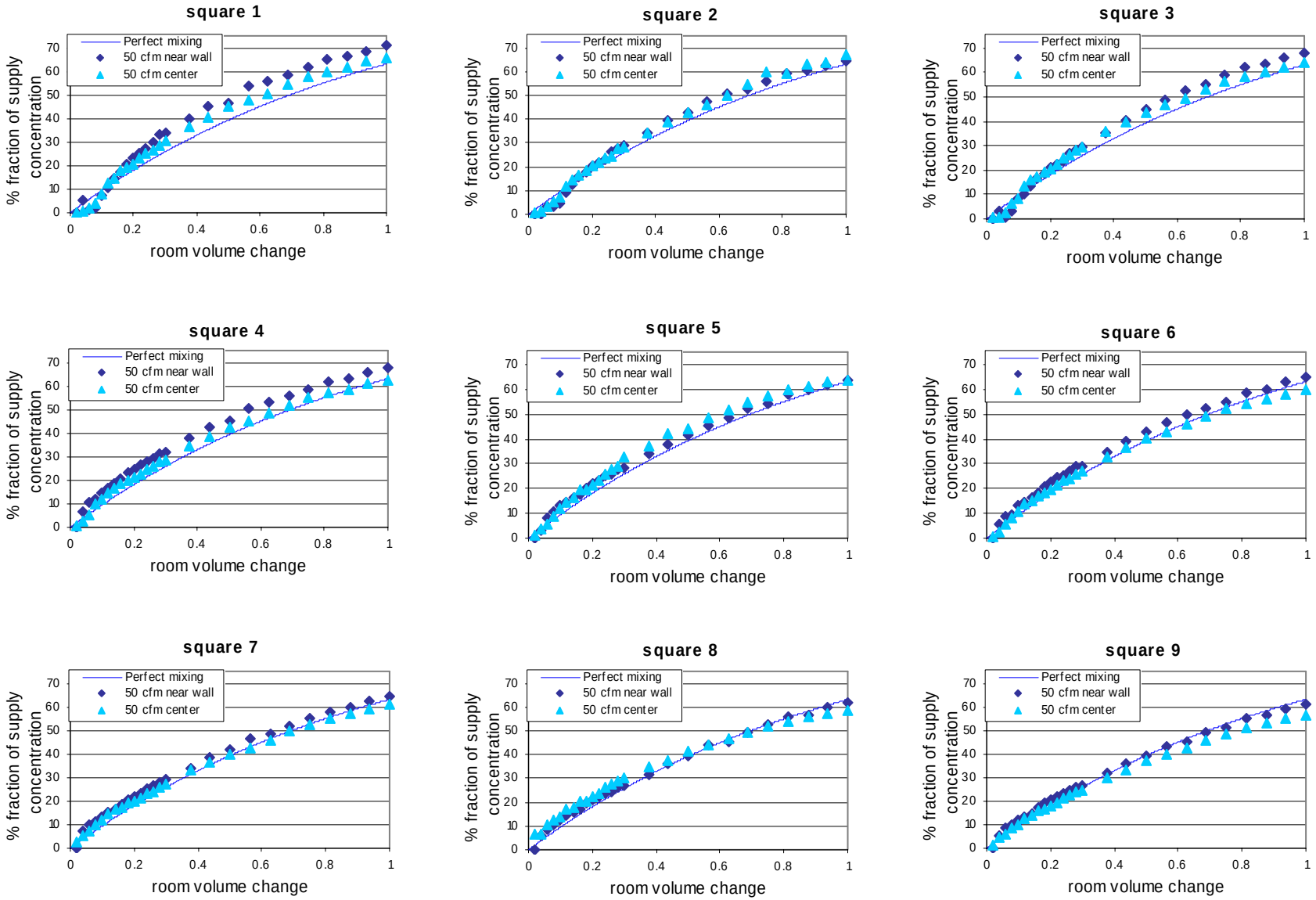

Figure 7.9: Cooling simulation, inlet up-outlet down, comparison between centerline and near the wall, 50 cfm, squares 1-9

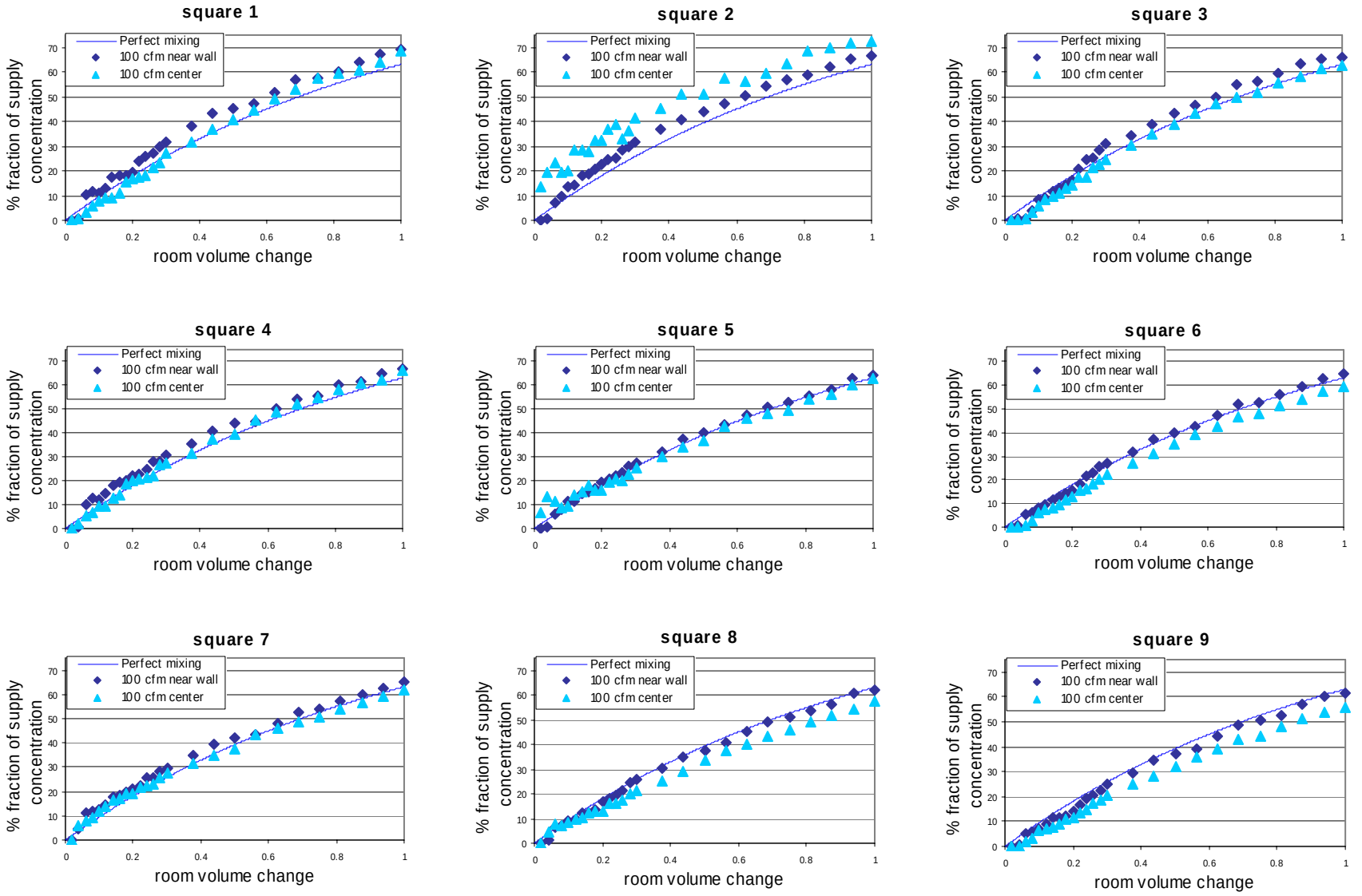

Figure 7.10: Cooling simulation, inlet up-outlet down, comparison between centerline and near the wall, 100 cfm, squares 1-9

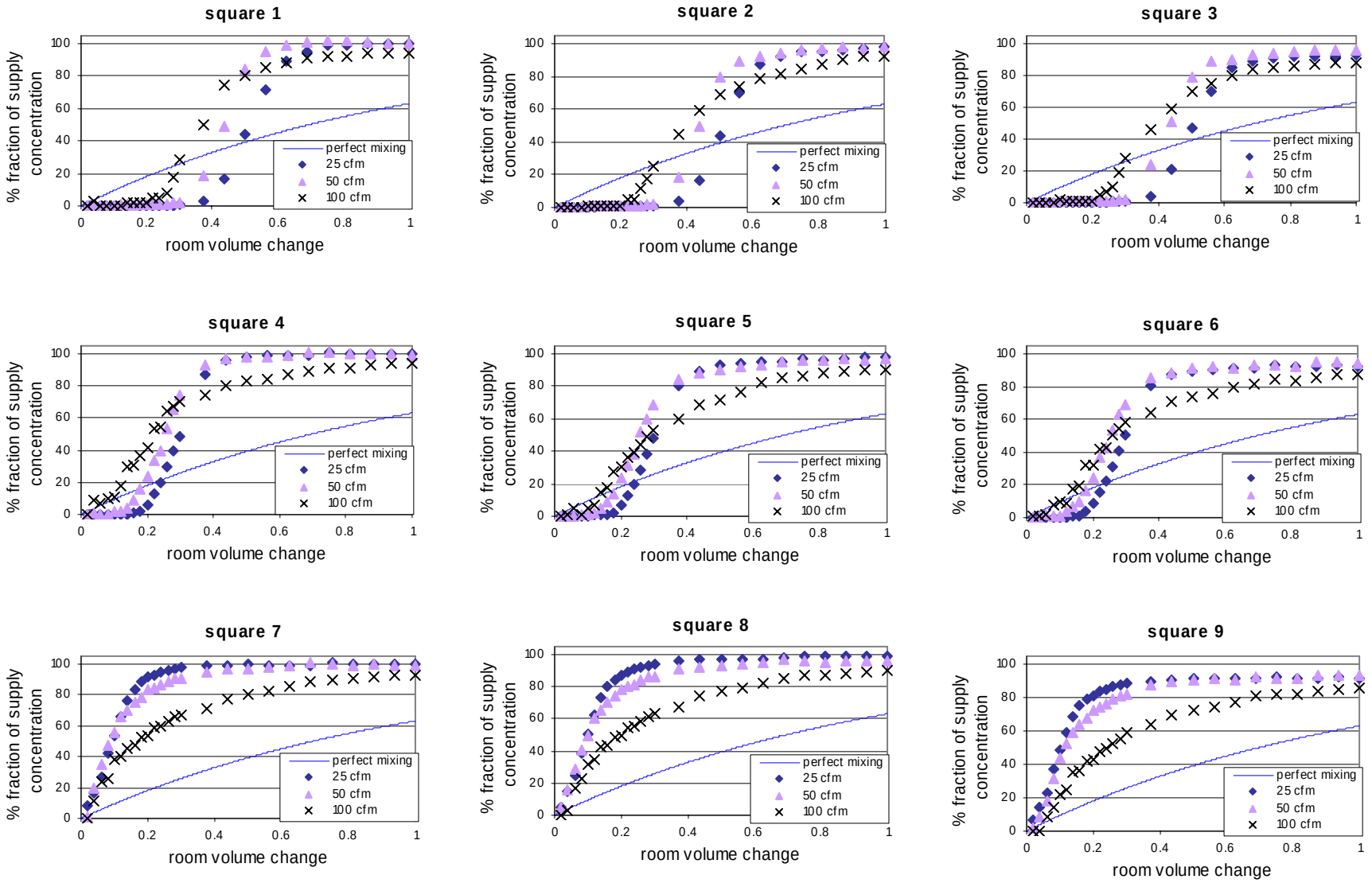

Figure 7.11: Cooling simulation, inlet down-outlet up, near the wall, squares 1-9

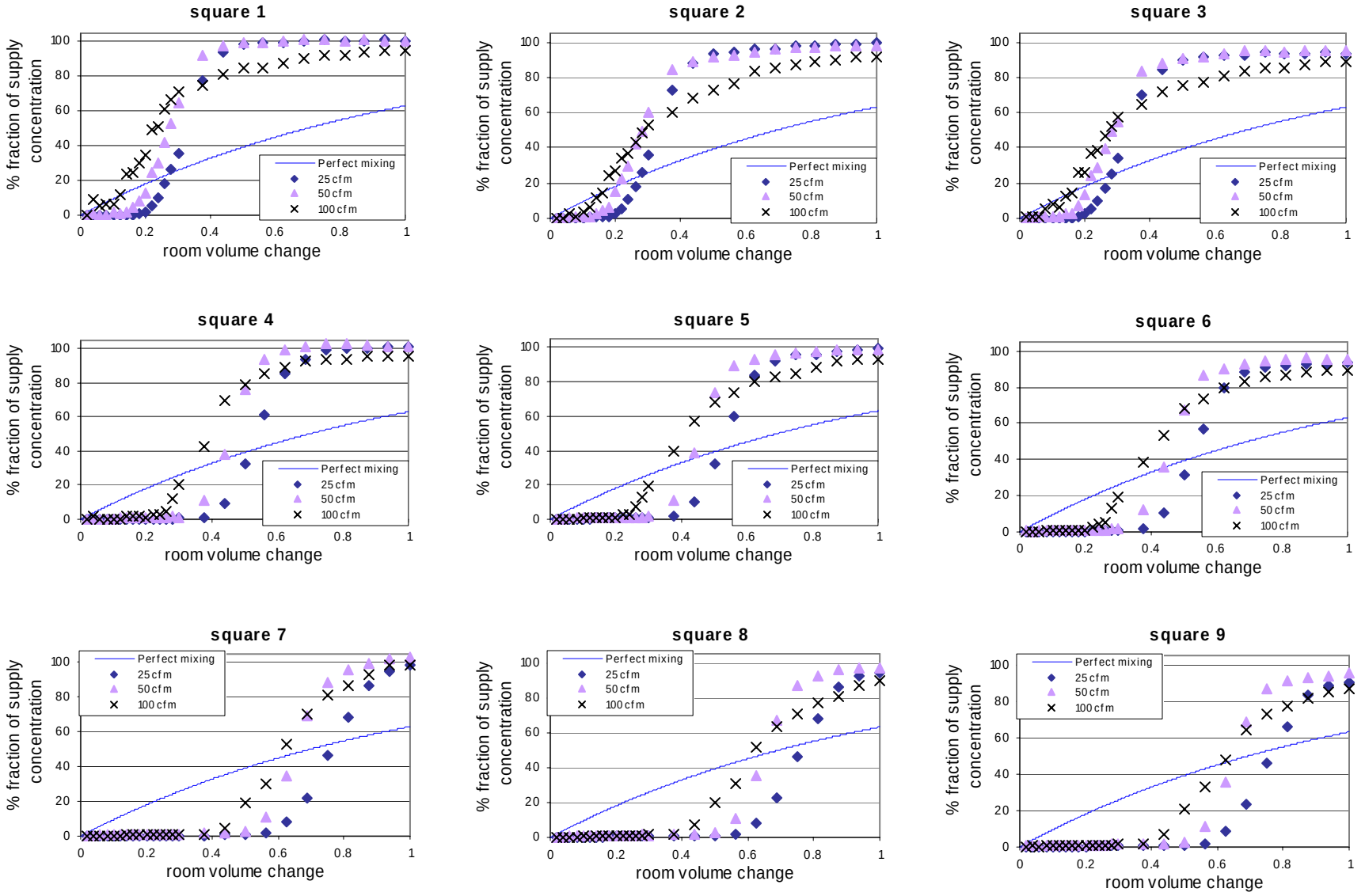

Figure 7.12: Heating simulation, inlet up-outlet down, near the wall, squares 1-9

References

ASHRAE Handbook of Fundamentals. 2001. ASHRAE, Atlanta, GA.

ASHRAE Standard 55-2004, *Thermal Environmental Conditions for Human Occupancy*, ASHRAE, Atlanta, GA.

ASHRAE, ANSI/ASHRAE Standard 70-1992, *Method of Testing for Rating of Performance of Air Outlets and Inlets*, ASHRAE Atlanta Georgia, 1991.

McNair, H.P. 1973. A Preliminary study of the subjective effects of vertical air temperature gradients. British Gas Corporation report No. WH/T/R&D/&3/94, London, U.K.

McNair, H.P. and Fishman, D.S. .1974. A Further study of the subjective effects of vertical air temperature gradients. British Gas Corporation report No. WH/T/R&D/&3/94, London, U.K.

Olesen, B.W., Schøler, M., Fanger, P.O. 1979. **Discomfort caused by vertical air temperature differences.** In: Fanger, P.O., Valbjørn, O. (eds) *Indoor Climate*, pp. 561-579, Danish Building Research Institute, Copenhagen, Denmark.

Thatcher, T. L., Wilson, D.J., Wood, E.E., Craig, M.J., and Sextro, R. G., 2002. *Turbulent Mixing of a Point Source Contaminant into a Large Room Using a Water-filled Scale Model.* Indoor Air, Volume 14, Pages 258-271. LBNL 50248

Titus, E. 2006. Strategies to Increase Residential HVAC Efficiency in the NothEast. National Association of State Energy Offices (NASEO) Contract #03-STAC-01

Tutu, N.K., Krishna, C.R., Andrews, J.W. and Butcher, T.A. 2003. Characterization of Airflows near the exit of HVAC registers using laser doppler velocimetry. Brookhaven National Laboratory Report BNL-71102-2003-IR, Upton, NY

Walker, I.S. and Modera, M.P., (1998), "Field Measurements of the Interactions between Furnaces and Forced Air Distribution Systems", ASHRAE Trans., Vol. 104, Part 1B, pp. 1805-1816. ASHRAE, Atlanta, GA. LBNL 40587